AFRL-ML-WP-TR-1999-4074

NEAR REAL-TIME MONITORING OF THIN-FILM MATERIALS AND THEIR INTERFACES USING EVANESCENT MICROWAVE PROBES

Massood Tabib-Azar

Manufacturing Instrumentation Consultant Co.
2762 Berkshire Road
Cleveland Heights, OH 44106

April 1999

Final Report for Period 15 May 1998 - 22 December 1998

Materials & Manufacturing Directorate
Air Force Research Laboratory
Air Force Materiel Command
Wright-Patterson Air Force Base, Ohio 45433-7734

NOTICE

When Government drawings, specifications, or other data are used for any purpose other than in connection with a definitely related Government procurement operation, the United States Government thereby incurs no responsibility nor any obligation whatsoever; and the fact that the government may have formulated, furnished, or in any way supplied the said drawings, specifications, or other data, is not to be regarded by implication or otherwise as in any manner licensing the holder or any other person or corporation, or conveying any rights or permission to manufacture, use, or sell any patented invention that may in any way be related thereto.

This report has been reviewed by the Office of Public Affairs (ASC/PA) and is releasable to the National Technical Information Service (NTIS). At NTIS, it will be available to the general public, including foreign nations.

This technical report has been reviewed and is approved for publication.

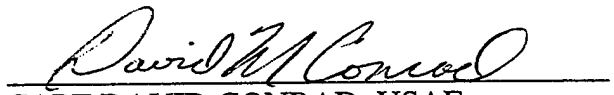

CAPT DAVID CONRAD, USAF
Project Engineer
Materials Process Design Branch
Manufacturing Technology Division

DR. STEVEN R. LeCLAIR
Chief
Materials Process Design Branch
Manufacturing Technology Division

"If your address has changed, if you wish to be removed from our mailing list, or if the addressee is no longer employed by your organization please notify AFRL/MLMR, Bldg. 653., 2977 P St., Suite 6, W-PAFB, OH 45433-7739 to help us maintain a current mailing list."

Copies of this report should not be returned unless return is required by security considerations, contractual obligations, or notice on a specific document.

REPORT DOCUMENTATION PAGE

FORM APPROVED
OMB NO. 0704-0188

1. AGENCY USE ONLY *(Leave Blank)*	2. REPORT DATE	3. REPORT TYPE AND DATES COVERED
	April 1999	Final 05/15/98 - 12/22/98

4. TITLE AND SUBTITLE

Near Real-Time Monitoring of Thin-Film Materials and Their Interfaces Using Evanescent Microwave Probes

5. FUNDING NUMBERS

C F33615-98-C-5136
PE 65502F
PR 3005
TA 05
WU AS

6. AUTHOR(S)

Massood Tabib-Azar

7. PERFORMING ORGANIZATION NAME(S) AND ADDRESS(ES)

Manufacturing Instrumentation Consultant Co.
2762 Berkshire Road
Cleveland Heights, OH 44106

8. PERFORMING ORGANIZATION REPORT NUMBER

MICC 005

9. SPONSORING MONITORING AGENCY NAME(S) AND ADDRESS(ES)

Materials & Manufacturing Directorate
Air Force Research Laboratory, Air Force Materiel Command
Wright-Patterson AFB, OH 45433-7734
POC: CAPT David Conrad USAF, AFRL/MLMR, (937) 255-8786

10. SPONSORING/MONITORING AGENCY REP NUMBER

AFRL-ML-WP-TR-1999-4074

11. SUPPLEMENTARY NOTES

12a. DISTRIBUTION/AVAILABILITY STATEMENT

Approved for Public Release; Distribution is Unlimited.

12b. DISTRIBUTION CODE

13. ABSTRACT

This is a Small Business Innovation Research (SBIR) Phase I Report

In this report we discuss a novel and very high spatial resolution (0.4 μm at 1 GHz) scanning method using evanescent microwave probe (EMP) techniques. In the course of this study the usefulness of EMP as a material characterization tool was demonstrated. Here we discuss the electronic and mechanical design methodology of EMP. Several novel design improvements were investigated and their effect on increasing the stability and reproducibility, on increasing the scanning speed, on confining the field pattern to increase the probe's resolution, on improving the signal-to-noise ratio (S/N) are discussed. Data acquisition, signal processing and image processing methods are also described. In this work, the output of the probe was calibrated to be able to offer quantitative results. With the calibrated probe, a large variety of materials ranging from dielectrics, semiconductors, metals, to biological specimens were scanned and the results are presented. We also suggest several future works for improving the performance of the probe. This final report is self-contained and it draws from many studies conducted using the EMP imaging technique.

14. SUBJECT TERMS

SBIR Phase I, Thin Films, Process Monitoring, Microwave, Materials, Laminates & Composite Materials, Metallurgy & Metallography, Crystallography.

15. NUMBER OF PAGES

90

16. PRICE CODE

17. SECURITY CLASSIFICATION OF REPORT	18. SECURITY CLASS OF THIS PAGE.	19. SECURITY CLASS OF ABSTRACT	20. LIMITATION ABSTRACT
Unclassified	Unclassified	Unclassified	SAR

Standard Form 298 (Rev 2-89)
Prescribed by ANSI Std Z239-18
298-102

1. Introduction

1.1 Motivation

Probing and imaging techniques are extremely important in material characterization. Most of these techniques employ electromagnetic fields with variations in the operating frequency being the only difference. Among these techniques, optical microscopy was first introduced, with human eyes playing a crucial part as the elegant sensor; other frequency ranges like microwave, infrared, ultraviolet, x-rays, γ-rays, and electron wave functions have also been successfully used for probing and imaging materials. Operating frequency determines the probe's performance, i. e., the spatial resolution, material sensitivity, penetration depth, speed of characterization, and operating environment. Therefore, each method (of a certain frequency) is suitable for specific application of material characterization.

The evanescent microwave probe, a relatively new member of the probes' family, bears some interesting features which make it a powerful probing and imaging technique for certain important applications. By its name, this probe operates in microwave range, which means it has the ability to measure a material's microwave characteristics (i. e., conductivity and permetivity); on the other hand, this probe takes advantage of evanescent field, which makes the resolution boost to the range of sub-micron.

Combining these two features, we can easily see the usefulness of this probe as a characterizing tool for the intermediate range of resolution, and its versatility in detecting features of a large variety of materials.

Here are some typical applications of evanescent microwave probe:

(a) Semiconductors

Non-destructive semiconductor characterization is important for measuring parameters whose values are unique to a sample, such as carrier concentrations, minor carrier life time, interface trap densities, and junction characteristics. Also, accurate characterization of surface states is crucial for maintaining performance and reliability of processes and devices in Very Large Scale Integration (VLSI). As the integration capability increased, the surface to volume ratio of device goes up, which requires the junctions be shallow and heavily doped. The determination of the depth of these junctions and their doping concentrations is becoming more and more important and requires more and more accurate characterization tools. Standard characterization techniques for junctions and surface states include junction staining, spreading resistance profiling, differential hall measurements, and transmission electron microscopy, but all of these methods are destructive. Also, the parameters they measured often vary from sample to sample. Scanning Capacitance Microscopy (SCM) can be used to measure surface states, it performs 2D profiling of carrier densities in shallow junctions and can potentially be used to directly measure device

capacitance, surface defects, interface trap densities and carrier recombination/generation rates. The interface trap densities are estimated by comparing high and low frequency C-V measurements. Quasi-static C-V measurements are not performed by the SCM because of inherent noise problems. Scanned microwave reflection coefficient measurements can provide all the above information and furthermore, it is a non-contact and non-destructive probing technique. Using the scanning evanescent microwave probe makes it also possible to non-destructively characterize defects, interface traps, non-uniformity, inclusions and junctions in semiconductors.

(b) Metals

For characterization of flaws in metals, the use of eddy currents is a popular method. However, with eddy currents it is difficult to detect planar cracks and laminations that lie in the plane of the eddy. Defect detection in intricately designed welds requires special coils and sensitive, multi-frequency eddy current instrumentation.. Using microwaves, on the other hand, delaminations within skin depth of the surface can be detected, as well as fine and shallow cracks on the surface of the metal. This method is easier to use than the eddy current probe for such applications. In addition, it can also be used for testing the integrity of brazed junctions, a welding joint, which bonds materials by heating them to a suitable temperature. These junctions are presently evaluated using x-rays. Gold is incorporated in the filler material to differentiate junctions from the background. The x-rays detect the gold

in the junction. Using the evanescent microwave probe, it is possible to develop a fast, inexpensive, and accurate inspection method that does not require a gold additive.

(c) Insulators

For testing insulators, evanescent microwave probing can be used to determine dimensions, moisture content, chemical composition, degree of aging, presence of voids, delaminations, cracks, and metallic inclusions of dielectrics and composites. To justify this, let us make a comparison between evanescent microwave testing and the popular ultrasonic testing technique: a) Electromagnetic waves have relatively high transmission coefficients across solid-air boundaries in comparison to ultrasound. b) The absorption coefficients of ultrasound for dielectrics are much higher than those of microwaves. c) The piezoelectric effect used in ultrasonic testing starts diminishing at higher temperatures and vanishes at Curie point, while microwave testing is not limited by temperature of the sample--it is non-contact and therefore is more suitable for high temperature testing. d) Large frequency variations with fixed amplitude are very easily obtainable for microwaves as opposed to ultrasound; such multifrequency operation provides us with an additional variable to analyze the response of the material. e) Ultrasound testing has a resolution of the order of 1mm, while evanescent microwaves can achieve a resolution of up to 1um by using high frequencies. All of the advantages shown above demonstrate the powerfulness of evanescent microwave as a probing technique for insulators as well.

(d) Biological tissues

For characterization of biological tissues, the use of evanescent microwave probe is also very attractive because the dielectric properties of biological tissues can vary greatly. The relative microwave permitivity of soft tissues, in the frequency range of 1-10GHz, varies from 5-50. The conductivities for these tissues vary from 1 to 500 S/m. These variations usually reflect the variations of physiological state, such as the change of temperature or humidity. Therefore, with the scanning evanescent microwave probe, we may obtain the images containing any information (for example, the thermal image), for a diagnostic use. In traditional imaging methods such as X-ray topography, images are basically determined by the variation in sample densities. In many cases, the change in physiological condition does not cause much change in density within the biological tissue. On the other hand, dielectric properties change with the physiological state of the tissue, thus making the evanescent microwave probe useful for diagnostic purposes and treatment.

From all of above, it is clear that evanescent microwave probe is a very versatile tool in detecting a wide range of materials. This technique has the following advantages:

1) It is non-destructive, non-contact, non-invasive.

2) No sample preparation is required.

3) It has relatively large mapping scale.

4) It is essentially a fast imaging technique.

5) It can be placed in all most any environment.

6) It can scan over moving object.

Table 1 gives a comparison between some commonly used characterization techniques. It shows that evanescent microwave probe can be used to fill the mid-range gap of resolutions with unique penetration depth. Methods with higher resolutions often suffer from one or more of the following problems:

1) Incompatible for detecting large-scale samples

2) Scanning time is limited by the frequency or bandwidth of associated electronics

3) Only suitable for samples of certain conductivity

4) Destructive sample preparation needed

5) Complicate equipment needed

6) Only useable at a limited temperature range

Again, we can clearly see that evanescent microwave probe can compliment the family of material characterizing probes by resolving many kinds of features in the range of 1um to 1cm near the surface.

Table 1 Comparison of some common methods for material characterization, with the evanescent microwave microscope. (Adopted from Ref. 17)

Method	Resolution	Conductivity Limits	Comments
STM[1]	Atomic level.	Good electron or ionic conductivity required.	No free electrons involved so can be conducted in air/liquid/vacuum. Field of view is only a few μm^2. 300 by 300nm area scan takes 10 min.
AFM[2]	Crystallized hard material: atomic. Biological: 2 nm.	No requirements on conductivity.	Surface preparation required. Both contact and non-contact methods exist.
Optical Microscopy[3,4]	1-10 nm	No requirements on conductivity.	For high resolution the probe needs to be a few nms from the sample. A 250μm x 250 μm scan takes 30 s.
SEM	100 nm.	Limited to materials that are conductive.	Vacuum sample preparation. Charging in non-conductive can be avoided by using thin metal layer. Expensive instruments.
X-ray[5]	5 μm (subμm with synchrotron).	No limitations.	Poor sensitivity to the surface. Sample preparation required. Expensive and huge equipment.
Evanescent Microwave	.4 μm at 1GHz	Penetration depth limits bulk probing in metals.	Good for large-scale mapping. Hot and moving samples can be imaged. No sample preparation. Can be used in air/liquid/vacuum.
Eddy Current[6]	50 μm.	Sample should be conducting.	Cannot detect planar cracks in the plane of the eddy. Complicated coil designs for some applications.
Ultrasonic[7]	Order of 1 mm.	No requirements.	Intimate coupling required due to poor transmission over boundaries. Not useful at high temperature.

1.2 Background

The classical spatial resolution limit to any instrument that is based on the propagation of electromagnetic fields is $\lambda/2$ (known as Abbe barrier). However, this limitation only holds for the "far field", which is the field at least one wavelength away from the source. In nature, this is the spatial version of "sampling theorem": to fully recover a point like signal, one has to recover all spatial frequency components of it. However, the evanescent waves decay exponentially in propagation. Therefore, they contain components of spatial frequency higher than $1/\lambda$. This is the fundamental reason why evanescent wave imaging exceed the Abbe barrier.

The first proposed optical imaging system taking advantage of the evanescent wave dates back to 1928, by Synge. His basic idea is to scan a point-source closely over an object to make sure the interaction through evanescent is strong enough. The early experimental efforts on evanescent microwave microscopy were given by Ash and Nicholls[8]. In 1972, they reported a spatial resolution of $\lambda/60$ for one dimension, and $\lambda/20$ for two dimension. A later development achieved a 0.1mm ($\lambda/2500$) spatial resolution. Evanescent fields are also used in other microscopy. For example, the near field electron wavefunctions used in scanning tunneling microscopy results in atomic resolution; near field optical scanning microscope may provide a resolution of nanometer.

Recently, as thin-film material (i. e., high temperature superconductor, novel semiconductors) becomes more important, evanescent microwave probes have attracted more attention. The unique penetration depth makes the evanescent microwave probe able to image sub-surface features as well as bulk properties; therefore, making it extremely powerful for thin-film material characterization. From 1993, the research groups[9-13] in University of California, Berkeley and University of Maryland (College Park) have been working on evanescent microwave probes. Both groups use resonant coaxial cable (with a very high Q) as their basic probe structure; and both employ a phase lock loop (PLL) to perform frequency modulation (FM) to improve the signal to noise ratio (S/N). In the Maryland group, they achieved a 20micron resolution and did research on quantitative imaging and sheet resistance mapping of superconductors. Their scanning speed is relatively fast (30 Hz), and the scan is non-contact. On the other hand, their setup includes a two meter long coaxial cable. The Berkeley group, have reported a 5micron resolution with planar scan and a 0.1micron resolution with perpendicular scan. Also, they performed a lot of research on superconductors and magnetoresistive materials. The major disadvantage of their probe is that the tip needs to make contact with the sample surface.

Our lab's research[14-17] on evanescent microwave probe dates back to 1989. Professor M. Tabib-Azar was one of the first people who came up with the idea of applying resonant electric dipole in near field microwave probe. In the previous

experiment setup, a micro-stripline resonator was used and carefully characterized. The output dependence on probe material, coupling strength, substrate permitivity and tapering were studied in detail. Qualitative mapping of conductivity was studied for various samples such as dielectrics and biological specimens, and some image processing techniques were also developed. The probe provided an 80microns resolution.

1.3 Objectives

This work explores the scanning evanescent microwave probe techniques. The usefulness of this probe as a material characterization tool will be further revealed, and its versatility in probing a large variety of features and materials will be ascertained. This work will, for the first time, from a systematic point of view, provide the electronic and mechanical design methodology for this probe. Some crucial problems that limite the probe resolution will be attacked. Several novel design improvements will be discussed. Their effects, such as better the stability and reproducibility, faster scanning speed, more confined field pattern, and higher signal to noise ratio (S/N), will be show in contrast with the previous probe setup. Data acquisition, signal processing and image processing methods will also be discussed.

In this work, the output of the probe is calibrated to be able to offer quantitative results. The implementation of the optical (or microwave) secondary probe for the distance compensation will be discussed. With the calibrated probe, a large variety

of materials ranging from dielectrics, semiconductors, and metals, to biological specimens are scanned and the results are presented. The optimal frequencies and other operating conditions for the samples will also be mentioned.

Also, the theoretical analysis of this probe will be carried out, and the circuit model will be set up. Finally, the problems that still exist will also be mentioned, followed by some thoughts on how to further improve the probing system.

2 The Evanescent Microwave Probe (EMP)

In this chapter the basic structure of the scanning evanescent microwave probe is described. The principle of the probe's operation is also discussed, and the circuit model of this EMP is set up for theoretical analysis.

2.1 Probe Structure

The evanescent microwave probe, as shown in figure 1, is composed of a stripline resonator with a fine steel tip of rectangular shape (25micron by 75micron), two Rogers Duroid 5800 substrates on one of which the microstrip line is fabricated, a short feed-line, and a interdigitated coupling capacitor. The stripline is designed to have a length of $\lambda/4$, and a 50 Ω characteristic impedance. The Duroid substrates are used to confine the field pattern and therefore improve the Q of the resonator. The resonator is coupled by a three-fingered interdigitated capacitor to the short feed-line. The feed line is connected to a RF circulator, which directs the input signal and the reflected signal to circulate in a predetermined direction so that only the reflected signal can be passed to the microwave signal power detector. By monitoring the voltage output of the detector, we can obtain the information of the reflection coefficient. In fact, for a relatively large range, the voltage output of the microwave detector has a linear relation with the reflection coefficient.

Previous researchers in our group did a lot of work in the EMP design. They studied the dependence of the probe's performance on parameters such as the substrate

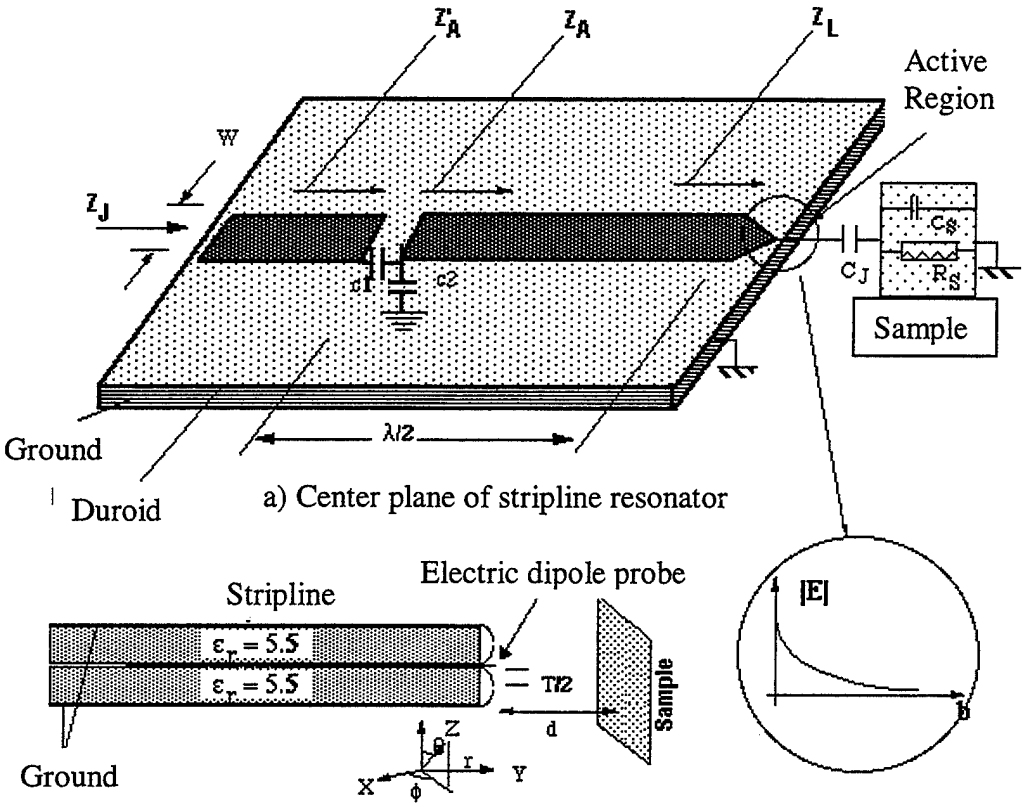

Figure 1 Stripline resonator and probe assembly.

permitivity, substrate thickness, coupling capacitance, and the taper angle of the probe tip.

After their work, several important improvements were made on the probe's construction, such as extruded tip, stripline structure, and probe housing. As a result, better resolution, stability and sensitivity were achieved. These improvements will be covered in details in Chapter 4.

2.2 Principle of Characterization

Unlike optical microscopes, the evanescent microwave probe usually take advantage of resonator structure to increase the signal-to-noise ratio by a factor of Q (200~2000). In this probe the resonator serves both as the evanescent field source and as a detector. Any interaction between the fields close to the tip of the probe and the surroundings lead to a change of the resonance characteristics. Figure 2 shows the shift in the resonance frequency of the probe when a metal sample is moved from far away to right in front of the tip. Figure 3 shows the different resonant frequencies when the probe is on top of different samples. These dependencies can be used to characterize materials.

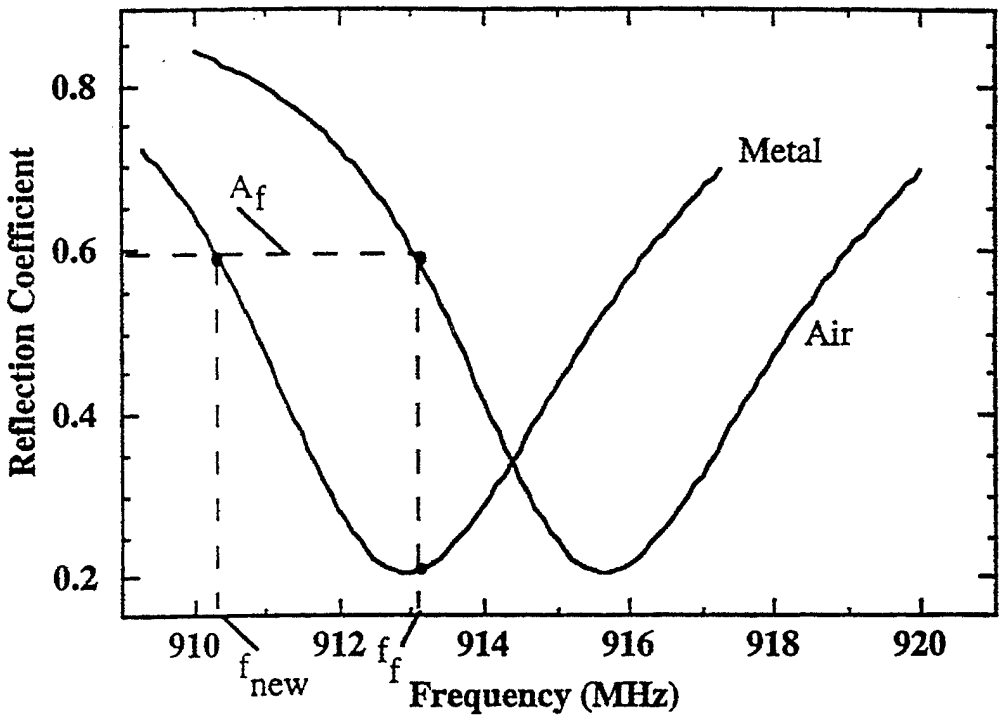

Fig 2 The resonant frequency shift of EMP when in presence of a metal sample.

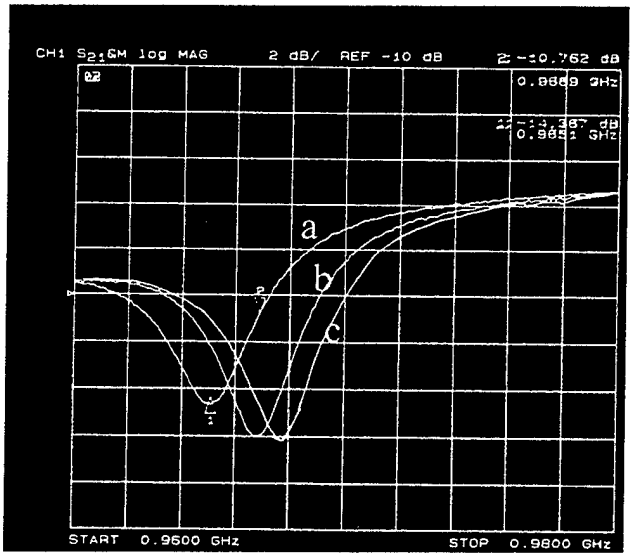

Figure 3 The EMP resonant frequency depends on the conductivity of samples. When put in the free space, the EMP has the highest resonant frequency (rightmost curve); when put in front of a insulator (glass), its resonant frequency shifts lower (the middle curve); when put in front of a metallic sample (copper), its resonant frequency shifts even lower (the leftmost curve).

Different materials display different microwave properties. More importantly, the conductivity and/or permitivity change from one material to another, which can change the EMP resonance frequency, thus changing the probe's output (proportional to the reflection coefficient). This means that the variations in local conductivity can also be detected. As the probe scans over an area of a sample, we can use the output of the probe to perform 2D conductivity mapping. Moreover, by manipulating the operating frequency, one can change the penetration depth of the evanescent field therefore producing a 3D conductivity imaging.

Variations in local conductivity of the sample can be due to many factors. In metal sample, the existence of defect, void and stress changes the conductivity locally. This change in conductivity can be detected by EMP. In semiconductor samples, the variation in carrier concentration, interface trap density, defects, and variation in layer thickness can all bring in some changes and therefore can be mapped. Some early works[2] on semiconductor characterization in our lab were well documented.

For insulators, their chemical and physical properties may cause a change in their permitivity, which also corresponds to a change in the reflection coefficient of the EMP. Permitivity change, in nature, is due to local variation in atomic (or molecular) polarizability. By classical electromagnetic wave theory[4], relative permitivity of a substance can be expressed as:

$$\varepsilon_r = 1 + \frac{N\alpha_T g}{\varepsilon_0} = 1 + \chi_e \quad (1)$$

where N is the number of atoms per unit volume, α_T is the atomic polarizability, and g is the ratio of the local electric field over the applied field. The above equation is called the Clausius-Mossotti relation for a spherically symmetric media. When frequency effects are also taken into account, it is known as the Debye equation. Electronic dipoles, ionic dipoles and permanent dipoles of the polar molecules all have contributions for the atomic polarizability:

$$\alpha_T = \alpha_e + \alpha_i + \alpha_d \quad (2)$$

Variations of cluster structure, density of impurities trapped charges, inherent spectral properties, and changes of physical conditions such as mechanical stress, temperature and moisture content may all vary the α_T (and therefore, the relative permitivity ε_r). All of these features can be detected and mapped by the probe.

To better understand the physics nature of probing, the concept of dipoles is used.[4] The probe may be used in two configuration: open-circuit probe (electric dipole), or short-circuit probe (magnetic dipole). When the probe is constructed as an open-circuit probe, the field lines at the end (tip) of the probe begin with high potential and end at the ground plate. The resonance occurs when the length of the probe is a multiple of $\lambda/2$. On the other hand, when the probe is constructed as a short circuit probe, the end of the probe is grounded, therefore haing the maximum current (just like magnetic dipoles). In the short circuit configuration, the length of the probe

needs to be $\lambda/4$. In both cases the effective length of the probe is larger than the physical length, and the effective length depends on the surroundings. When the sheet resistance of the sample increases, the boundary condition of the resonator tends to change from short circuit to open circuit. As a result, the probe changes from a quarter wavelength resonator to a half wave length resonator, and the resonance frequency shifts to a higher frequency.

2.3 Circuit Model of the Probe[18]

Typically, the resonance behavior of the simplest resonator can be described by a second-order equation. The microstripline or stripline EMP has a very complex frequency response (usually more than one pole). However, since the probe is only operated near one resonance peak, which has a very high Q (>1700), it is reasonable to model the resonator as a second order system by a LCR circuit. To describe the microstripline or stripline probe, which is in nature an open circuit transmission line, a series resonant circuit is used. Figure 4a shows the equivalent lumped element series LCR resonant circuit. For simplicity, conductors and insulators are modeled with different circuits as shown in Figure 4b and 4c. Here we will see how the probe's output (reflectance, in nature) is related to the electric characteristic of the sample. The derivation for semiconductors is pretty similar, though the final expression will be quite complex and not of illustrative use.

In both Figures 4b and 4c, the C_c stands for the capacitance of the air gap between the probe tip and the sample. C_c couples the electromagnetic properties of the sample to the LCR circuit; while the C_s and R_s model the capacitance and shunt resistance contributed by the sample of permitivity ε_s and conductivity σs.

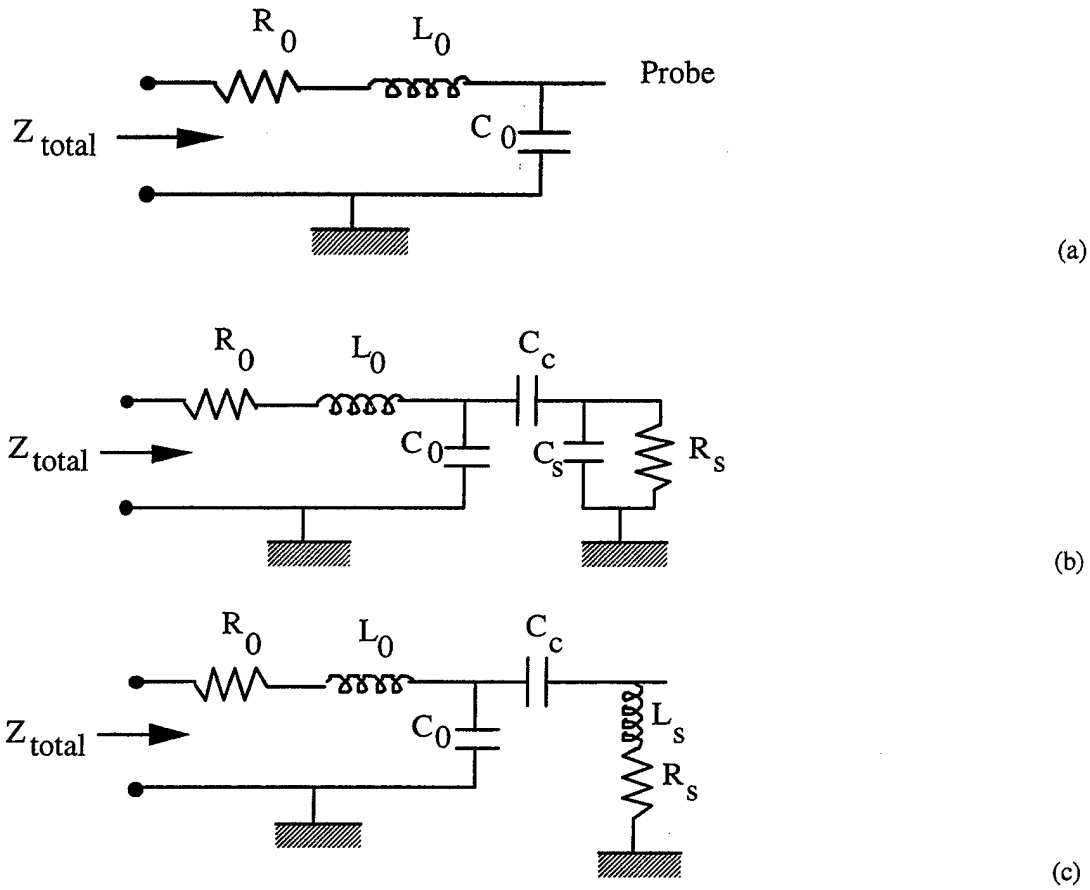

Figure 4 Circuit Models of EMP

(a) Series of lumped LCR model of the evanescent microwave probe.
(b) Circuit model in presence of an insulating sample.
(c) Circuit model in presence of a conducting sample.

In Figure 4b and 4c, the total impedance of the sample-coupled stripline resonator can be written as:

$$Z_{total} = R_0 + \frac{G_{eff}}{G_{eff}^{\ 2} + \omega^2 C_{eff}^{\ 2}} + j\omega\left(L_0 - \frac{C_{eff}}{G_{eff}^{\ 2} + \omega^2 C_{eff}^{\ 2}}\right) \tag{3}$$

where L_0 is the unit-length inductance of the stripline; ω is the angular frequency; C_{eff} and G_{eff} is given by the following equations:

For insulators:

$$C_{eff} = C_0 + \frac{C_c C_s}{C_c + C_s} \tag{4a}$$

$$G_{eff} = G_s\left(\frac{C_0 + C_c}{C_s + C_c}\right) \tag{4b}$$

For conductors:

$$C_{eff} = C_c \frac{C_c}{\omega^2 C_c^{\ 2} R_s^{\ 2} + (L_s C_c \omega^2 - 1)^2} \approx \frac{C_c + C_0}{\omega^2 C_c^{\ 2} R_s^{\ 2} + 1} \approx C_c + C_0 \tag{5a}$$

$$G_{eff} = G_s \frac{\omega^2 C_c^{\ 2} R_s^{\ 2}}{\omega^2 C_c^{\ 2} R_s^{\ 2} + (L_s C_c \omega^2 - 1)^2} \tag{5b}$$

The parameters of the sample (C_c, C_s, L_s, R_s) can be estimated by following equations:

The air gap (coupling) capacitance is given by: $C_c = \varepsilon_0 A_{eff} / d$

where A_{eff} is the effective area of the coupling capacitor, taken into account the fringing fields, d is the distance between the probe tip and the surface of the sample.

The sample capacitance is given by: $C_s = \varepsilon_s A_{eff} / \xi$

where A_{eff} is the same as above, ε_s is the permitivity of the sample, and ξ is the skin depth or the decay length of the electromagnetic field at the tip of the probe, depends on which is smaller.

The skin depth is given by: $\delta = 1/\sqrt{\pi f \mu_1 \sigma_s}$, where $\sigma_s = q\mu_2 n$, μ_1 is the permeability, μ_2 is the carrier mobility, σ_s is the conductivity, and n is the carrier concentration.

The sheet resistance is given by $R_{sheet} = 1/\delta\sigma_s$, this allowing the sample resistance to be written as: $R_s = l_{eff} /(w_{eff}\delta\sigma_s)$

where l_{eff} and w_{eff} are effective length and effective width of the cross section of the tip, usually $l_{eff} = w_{eff}$.

To see how the shift in resonance frequency depends on the electromagnetic properties of the sample, one may rewrite equation (3) in the following form:

$$Z_{total} = R' + j(\omega L' - \frac{1}{\omega C'}) \qquad (6)$$

for insulators (figure 4.3),

$$R' = R_0 + R_s \frac{C_c(C_c + C_0) - C_0 C_s}{(C_c + C_0)^2} \tag{7a}$$

$$L' = L_0 \tag{7b}$$

$$C' = C_0 (1 + \frac{C_c C_s}{(C_c + C_0) C_0}) \tag{7c}$$

for metals (figure 4.2),

$$R' = R_0 + R_s C_c \omega^2 (C_c - C_0) \tag{8a}$$

$$L' = L_0 + \frac{L_s C_c^{\,2}}{(C_c + C_0)^2} \tag{8b}$$

$$C' = \frac{C_c + C_0}{\omega^2 C_c^{\,2} R_s^{\,2} + 1} \approx C_0 + C_c \tag{8c}$$

In both cases, the resonance frequency of the stripline resonator (coupled with sample) is given by: $\omega' = \sqrt{\frac{1}{L'C'}}$ (9)

which is very close to the intrinsic resonance frequency $\omega_0 = \sqrt{\frac{1}{L_0 C_0}}$, where L_0 and C_0 are the inductance and capacitance of the stripline per unit length. Therefore, we can treat the presence of sample as a small perturbation. By factoring out ω_0, we have:

for insulators,

$$\omega' = \omega_0 \sqrt{\frac{1}{(1+\frac{C_s C_c}{C_0(C_c+C_s)})}} \approx \omega_0 (1 - \frac{1}{2}\frac{C_s C_c}{C_0(C_c+C_s)}) \tag{10a}$$

for metals,

$$\omega' = \omega_0 \sqrt{\frac{1}{(1+\frac{L_s C_c^{\,2}}{L_0(C_c+C_0)^2})(1+\frac{C_c}{C_0})}} \approx \omega_0 (1 - \frac{1}{2}\frac{C_c}{C_0})(1 - \frac{C_s C_c}{C_0(C_c+C_s)}) \tag{10b}$$

The quality factor Q of the resonator, which is defined by $Q = \frac{Z}{R} = \sqrt{\frac{L}{C}}/R = \frac{\omega L}{R}$, also changes with the presence of the sample.

In terms of the quality factor Q, the total impedance can also be written as follows:

$$Z_{total} = R'\left[1 + jQ'\left(\frac{\omega}{\omega_0} - \frac{\omega_0}{\omega}\right)\right] \tag{11}$$

This equation will be used for resolution calculation in chapter 4.

To relate the reflectance of the microstripline resonator to its impedance, we have:

$$S_{11} = \frac{Z_{total} - Z_0}{Z_{total} + Z_0} \tag{12}$$

where S_{11} is the reflectance, and Z_0 is the characteristic impedance of the feedline. Up to now, it is clearly shown that the probe output depends on the shift of resonance frequency (ω) and the change of resonator's quality factor (Q), therefore further depends on the electromagnetic parameters (σ and ε).

2.4 Probe Design

For completeness, some works done by previous researchers[8] in our group and their conclusions on the probe design are included here.

Probe material:

Reinforced Teflon Duroid of two different permitivities (2.2 and 10.8) are used as the substrate. The 2.2 substrate has low water absorption and low thermal conductivity, while the 10.8 substrate reduces probe size and improves resolution. Both substrates had rolled copper foils for low resistivity and smooth metal surface.

Coupling strength:

The interdigitated capacitor which couples the feed line to the resonator affects the resolution. Over-coupled resonators have lower Q, while under-coupled resonators deteriorate the coupling strength, which also results in lower Q. A critical coupling exists.

They also studied the tapering effect of the probe. Since the tip of the probe has been changed to a protruding wire, their conclusion is not applicable and therefore is no longer included in this report.

3 The EMP System

This chapter is about the experimental setup of the evanescent microwave probe (EMP) system. It exposes in detail the equipment, data acquisition, control, and image generation.

3.1 The System Setup

The schematic of the experimental setup is shown in figure 5.

The key element of the EMP system is a stripline microwave probe resonating as an electric dipole, as shown in figure 1. The microstripline is designed to have a 50Ω characteristic impedance, and is coupled with a short feed line. Both the microstripline and the feed line, as well as the two substrate layers, are tightly covered by a aluminum housing, with only the tip of the probe protruding through a hole in front of the housing. The feed line is then connected to port 1 of a three-port circulator. Port 2 of the circulator is connected to a RF signal generator which serves as the microwave signal source. Port 3 of the circulator is connected to a crystal microwave detector. The detector's output is a voltage that has a linear relationship with the power of the reflected wave. This output from the crystal detector is fed to a series of amplifiers. The circulator and detector are mounted on top of the aluminum housing, which is fastened to the z-direction transition stage supported by a metallic frame. Under that housing, there is a plate serving as a sample holder, which can be tilted to make the surface of the sample perpendicular to the tip of the probe, thus

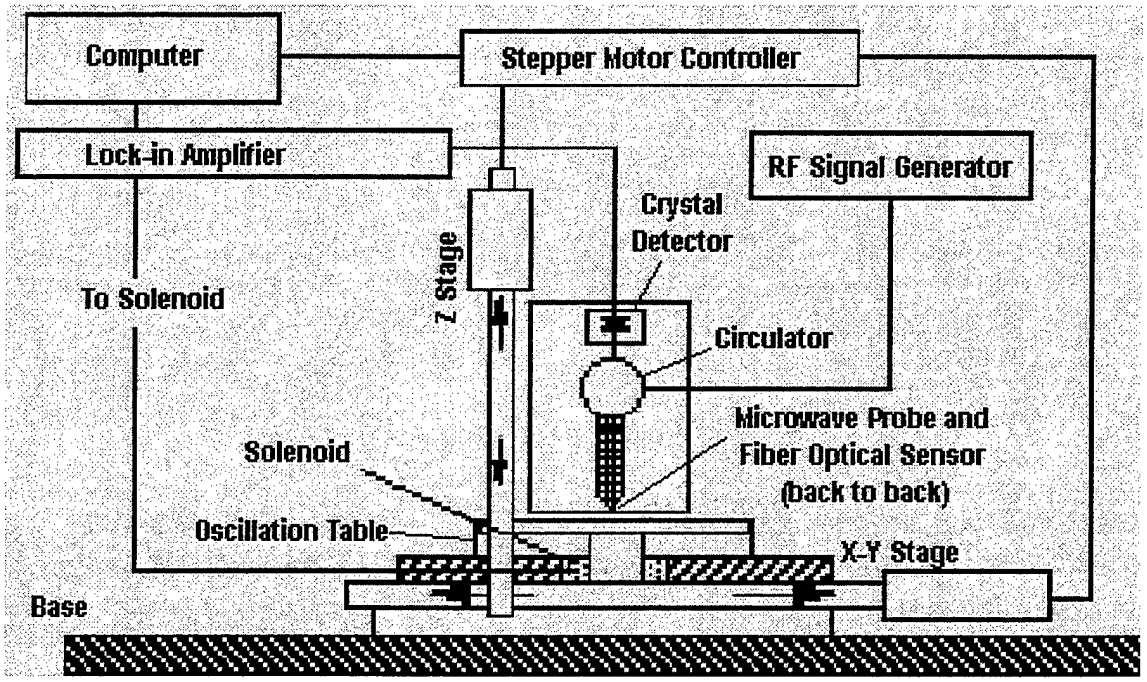

Fig 5 Schematic of the EMP system

ensuring that during the scan, the distance between the probe tip and the sample is approximately constant. The sample holder is seated on a x-y stage. A PC is used to control the scanning of the x-y stage as well as the z stage distance adjustment. Also, the PC is used to control the RF signal generator and the data acquisition (DAQ) board.

The basic setup is stated as above and is shown in figure 6. For different probing experiments, other devices can be added as required. When one needs to perform a synchronous detection to improve the signal to noise ratio (S/N), a piezo-crystal oscillator and its power source are used. A lock-in amplifier is also used to pick-up the modulated signal. When samples of a large area are scanned, one can not eliminate the distance variation by simply tilting the sample holder. In this case, a fiber optic distance sensor is mounted in the front of the aluminum housing, and its output is fed back to the PC for distance compensation. When multi-frequency detection is performed, both a 1GHz probe and a 10GHz probe are installed back to back inside the aluminum housing. When the photon induced carrier concentration variation of semiconductor is studied, a strong light source, focusing lenses, and light-chopper are employed. When one wants to perform a C-V measurement for semiconductor samples, a DC power source and an inductor are added to the setup. When the frequency property of the probe is studied, a network analyzer is also included. From all of above, we may see the simplicity and versatility of this setup. It can be easily modified for other applications.

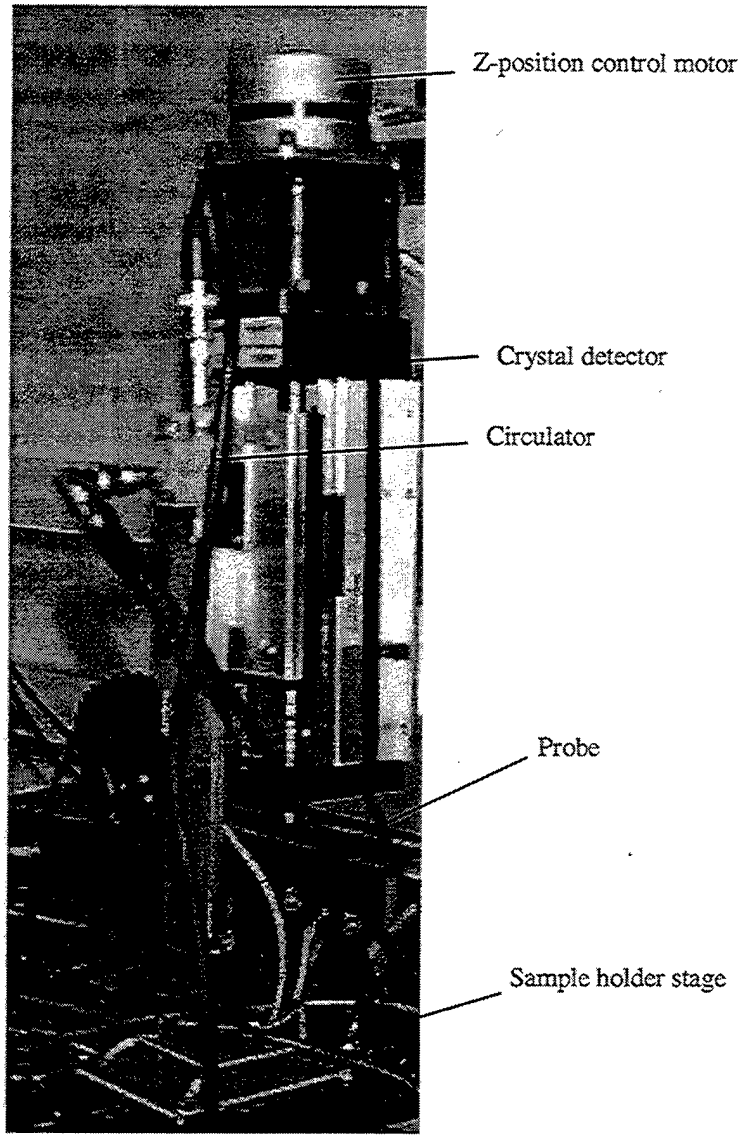

Figure 6 Typical experiment setup for the EMP imaging system.

The detectors we use for the probes are the HP8472B low biased Schottky barrier detectors (Herotek's DDS018 was once used also). They are square law detectors and have a sensitivity greater than 500mV/mV, and they can be operated from 10MHz to 18GHz.

The circulators that are used are the RADC-940-960M-S3-20W, the RADC-9.8-10.2-S3-5W from Raditek, and the M3C0890 from Midisco. At both the 1GHz and 10GHz frequencies, these circulators provide 20dB isolation. The bandwidth of the 1GHz circulator is 40MHz, while the bandwidth of the 10GHz circulator is 400MHz.

A Fluke 6060B synthesized RF signal generator is used to provide the input for the 1GHz probe. It may be operated from 10KHz to 1040MHz, and the frequency is accurate to 1Hz. For the 10GHz probe, a HP8684B signal generator, which has a operating frequency range of 5.4 to 12.5 GHz, is used as the signal source. To study to probe's frequency behavior, the HP 8410B (network analyzer), the HP8412A (phase magnitude display module), and the HP 8414A (polar display module) are also used when characterizing the probe.

The housing of the probe is made of aluminum for shielding purpose. Two apartments are next to each other, separated by an aluminum plate, for the 1GHz probe and 10GHz probe respectively. On top of the housing, a SMA male connector

is mounted (connected to the circulator), while in the bottom of the housing, a 5mm*1mm hole is made for tip protrusion.

The sample holder is made up of two closely spaced metallic plates (for grounding). Two micron-meters are installed at two corners of the plates. On the other side, a small metallic ball is seated in a pit between the two plates, along with the two micron-meters, making the top plate tiltable. Several springs are used to hold the two pieces together.

The X-Y-Z stage is a linear positioning table (Model M1-102404) from Kollmorgen. It is fitted with three stepper motors and three integrated-stepper-motor-controllers (SMC501PSA). The motors are used to drive the X-Y-Z stage for three-dimensional motion. The SMCs provide the low-level control over the stepper motors. Each of the SMCs has a RS232 port which enable them to communicate with PC for high level control. They are 'daisy-chained' onto the single RS232 port of the PC. On the PC, the programming tasks include initializing the SMCs, setting up the configurations, driving the motors, and powering down the SMC. All of these tasks are done by writing special ASCII codes to the RS232 port. The SMCs takes care of all the acknowledgements and inter-communications.

For asynchronous probing, a Tektronix AM 502 Differential Amplifier is used, while for synchronous probing, a Model 5186 Preamplifier and Model 5110 Lock-in

Amplifier from EG&G Princeton Applied Research are used. The amplified signal is then further amplified and digitalized by the DAQ board from National Instrument. To communicate with instruments without the RS232 port but with GPIB488 port instead (i. e., the Fluke signal generator), the GPIB488 Board from National Instruments is also installed on the PC.

3.2 Image Generation

As far as software is concerned, the LabView and GPIB Handler from National Instruments are currently used for control and data acquisition, although QuickBasic is used before. Matlab is used for image generation. The basic idea of generating 3-D images or 2-D pseudo-colored image is to assign a color value to small voltage (output) ranges. The voltage data is converted to a set of three numbers representing red, green and blue, which can be used to generate a portable pixel map. Matlab has many standard algorithms and functions for image processing (i. e., contrast enhancement, spatial filtering, deconvolution, etc.)

4. Performance Improvements of EMP Imaging System

In this chapter, we present several important techniques used to improve the probe's performance, such as confining the electric field pattern, increasing system signal-to-noise ratio, distance compensation, accurate position registration, speeding up the scanning, and introducing the graphic interface.

4.1 Resolution Improvement

4. 1. 1 General consideration

From figure 2 and figure 3, one can see that when the microwave probe is placed in the vicinity of a sample, the reflection coefficient of the probe changes by a certain amount, which depends on the probe-sample distance and the conductivity of the sample. This change is detected by the crystal detector, and it is then amplified to give the probe's output. The amount of this change $\Delta\Gamma$ can only be detected when it is larger than the combined noise level of the circulator/detector/amplifiers system, or in other words, S/N equals unity.

There are several different operation modes to perform EMP imaging:

a) Operate at a fixed frequency f_{fix}, measure the amplitude changes

b) Operate at a fixed amplitude, measure the frequency shifts

c) Operate at fixed frequency and amplitude and measure the changes of the probe-sample distance (like in STM)

To analyze the principal factors that affect the resolution (both spatial resolution and conductivity resolution) of the EMP, we hereby discuss mode a). Not only because our treatment can be generalized to other modes, but also because it gave us best resolution. The experimental comparison of different operation modes is included at the end of this section.

The detected signal $\Delta\Gamma$ can be expressed as:

$$\Delta\Gamma \approx \left[\frac{\Delta\Gamma}{\Delta f}\right]_{f_{op}} * \Delta f \tag{13}$$

where the f_{op} is the frequency of operation.

We denote the slope $\left[\frac{\Delta\Gamma}{\Delta f}\right]_{f_{op}}$ by S_x, which is the sensitivity of the resonator at f_{op} and approximately proportional to the quality factor Q.

Furthermore, the minimum detectable signal (MDS) is defined as the smallest input signal that produces an output equal to the output-referred rms value of the noise (V_{nrms}). When probing the changes of conductivity, $MDS = \Delta\sigma_s$. Note that $\Delta\Gamma/\Delta f = (\Delta\Gamma/\Delta\sigma_s)(\Delta\sigma_s/\Delta f)$, one may rewrite the minimum detectable signal as:

$$MDS = \Delta\sigma_s = \frac{V_{nrms}/V_{in}}{S_x S_f} \tag{14}$$

where $S_f = \Delta f / \Delta \sigma_s$. S_f denotes the frequency shift of the resonator due to per unit change in sample conductivity. S_f is determined by the strength of physical interaction between the sample and the probe via the evanescent field. Similarly, for non-magnetic insulator, the minimum detectable change of permitivity $\Delta\varepsilon_s$ is also given by formula (15), with S_f is re-defined as $\Delta f/\Delta\varepsilon_s$ correspondingly.

From equation (15), it is clear that to make the minimum detectable signal as small as possible, the following improvements should be made:

a) Maximize S_x.

   S_x is directly related to the Q value of the resonator. Therefore, Q should be maximized.

b) Maximize S_f.

   This requirement suggests short distance between the sample and probe is needed to ensure strong enough interaction.

c) Maximize V_{in}/V_{nrms}

As all other instruments, high Signal-to-Noise ratio is always desired. This shows the advantage of synchronized measurement (distance modulation) over asynchronized measurement at DC.

In the following sections techniques employed to achieve these improvements are discussed in details.

4. 1. 2 Techniques to Confine the Field Pattern

To improve the spatial resolution of the EMP, it is rather straightforward to confine[19] the electric field to a small local area; more over, for improving the conductivity resolution, it is also desirable to confine the evanescent field for a higher Q value. Three methods have been used to achieve this goal: stripline configuration, metallic housing, and tip tapering.

a) Stripline structure

For previous a version of the EMP, a microstripline type of probe was used. To obtain higher a Q value, a stripline resonator[20] is now in use. Figure 7 shows the frequency shifts of the microstripline resonator and the stripline resonator in presence of a metallic sample. By comparing these two curves, we may see that although the frequency shift of the stripline resonator is a little smaller than that of the microstripline, the stripline resonator has a high Q value, and the output (shown as the differences between with and without sample) is larger.

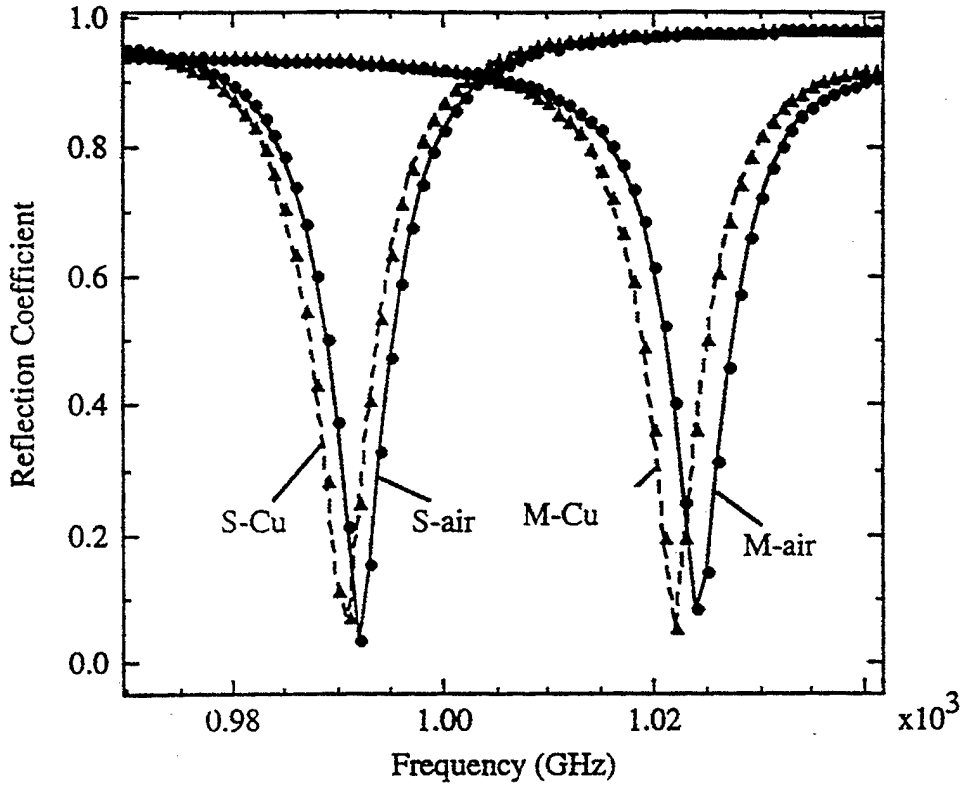

Fig 7 Experimental spectra of stripline (S) and microstripline (M) resonators with tapered tip located near a copper sample (S-Cu and M-Cu) and in air.

b) Metallic housing.

Metallic housing is used for several purposes:

- It can electro-magnetically shield the probe;
- It can provide perfect grounding;
- It serves as a robust mechanical support, which is very important for exact positioning;
- It confines the direction of evanescent wave propagation, localize the field;
- When used for multi-frequency application, it can eliminate the interference of the RF signals from different probes.

Fig. 8 shows the simulation result of the housing effect in limiting the evanescent field pattern[21]. The simulation is done with the SONNET finite element method.

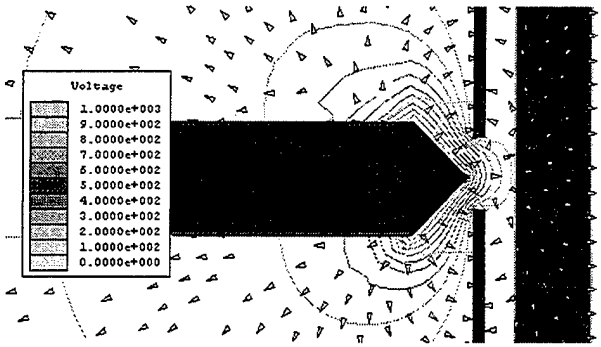

(a)

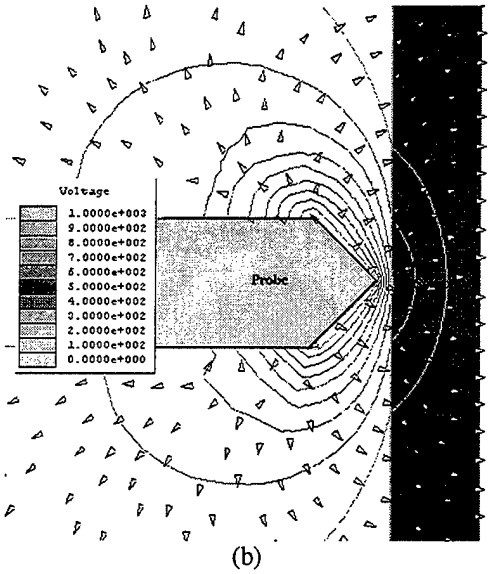

(b)

Figure 8 Simulations show the effect of metallic housing on limiting the electro-magnetic field

(a) Confined field near the aperture of the aluminum housing.
(b) More diffusive field in the open space.

c) Tip tapering[22]

The tip geometry is the major factor that determines the spatial resolution of EMP. Several methods have been tried to obtain better probe tips.

- Stainless steel tips prepared by wire cutter or by scalpel knife

  A typical image of these tips is shown in Fig. 9a. As one can see, the tip does not have a very smooth shape, and consequently makes the field pattern more diffusive; also, it is almost impossible to reproduce a good tip since each cut makes a tip with a different shape.

- Stainless steel tips are prepared by breaking a wire (20micron diameter) with a pulling force.

  A typical image of these tips is shown in Fig. 9b. The effective size of this tip is smaller than the cut ones. After simply chemical etching to clean the debris, the shape of this type of tip is also better defined. As a matter of fact, this tip gave us the best spatial resolution up to now and is still in use.

- Tungsten tips etched by an electrochemical method

  Fig. 9c shows the image of such a tip etched from a tungsten wire of 250micron in diameter. The etching setup is shown in Fig. 10. These type of tips have the best tip-shape, and can go down to an atomic size. For the time being, because tungsten wires of small diameter (<20micron) are very soft and easy to deform, we use only a 250micron wire for preparing

tips. Although consequently the resolution of this "STM" like tip is not as good as the "pulled" tip, it should be the way that will give us the best tip in the near future.

The resolution comparison of these tips is shown in Fig. 11. With each tip, we scanned over a 25μm by 125μm metallic wire, along the direction of the 25μm edge.

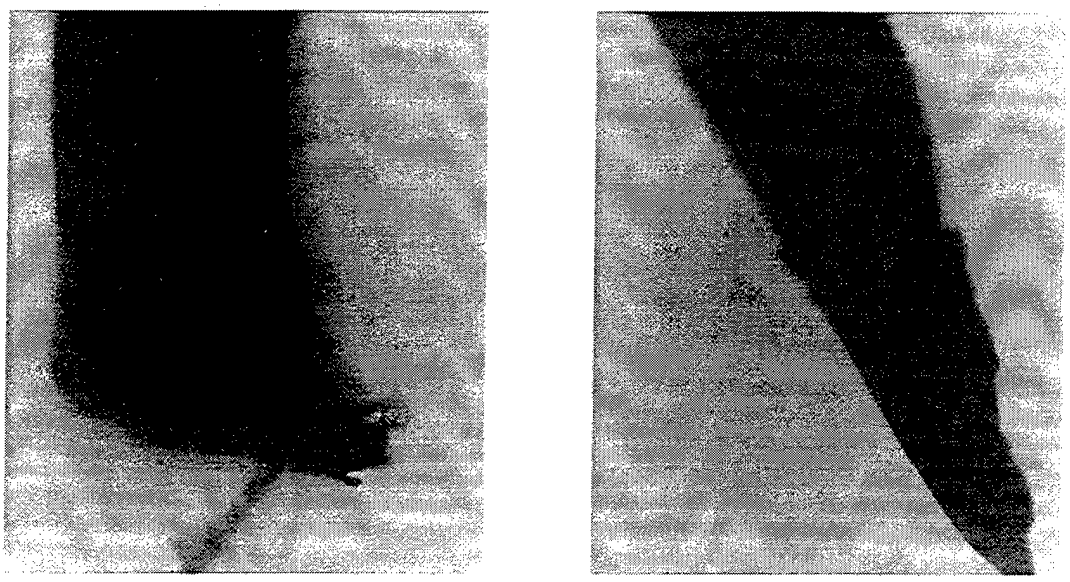

(a) (b)

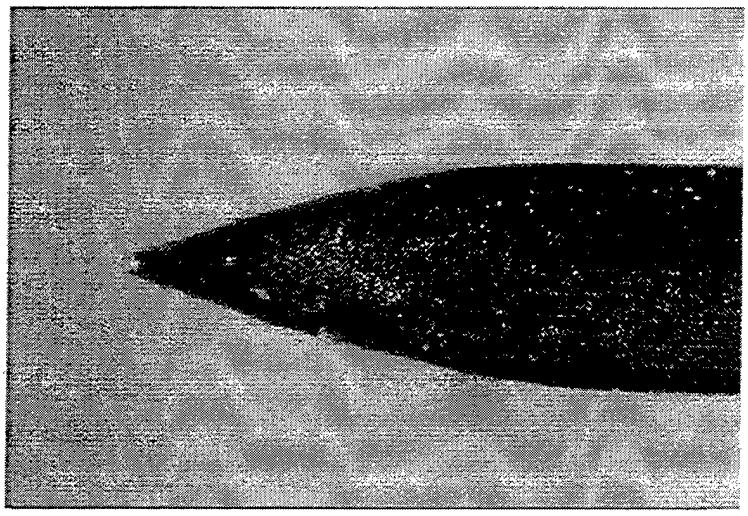

(c)

Figure 9 Optical image of tips prepared by different techniques.

(a) Tip prepared by exactor knife.
(b) Tip prepared by pulling force and chemical cleaning.
(c) Tip prepared by electro-chemical etching.

(d)

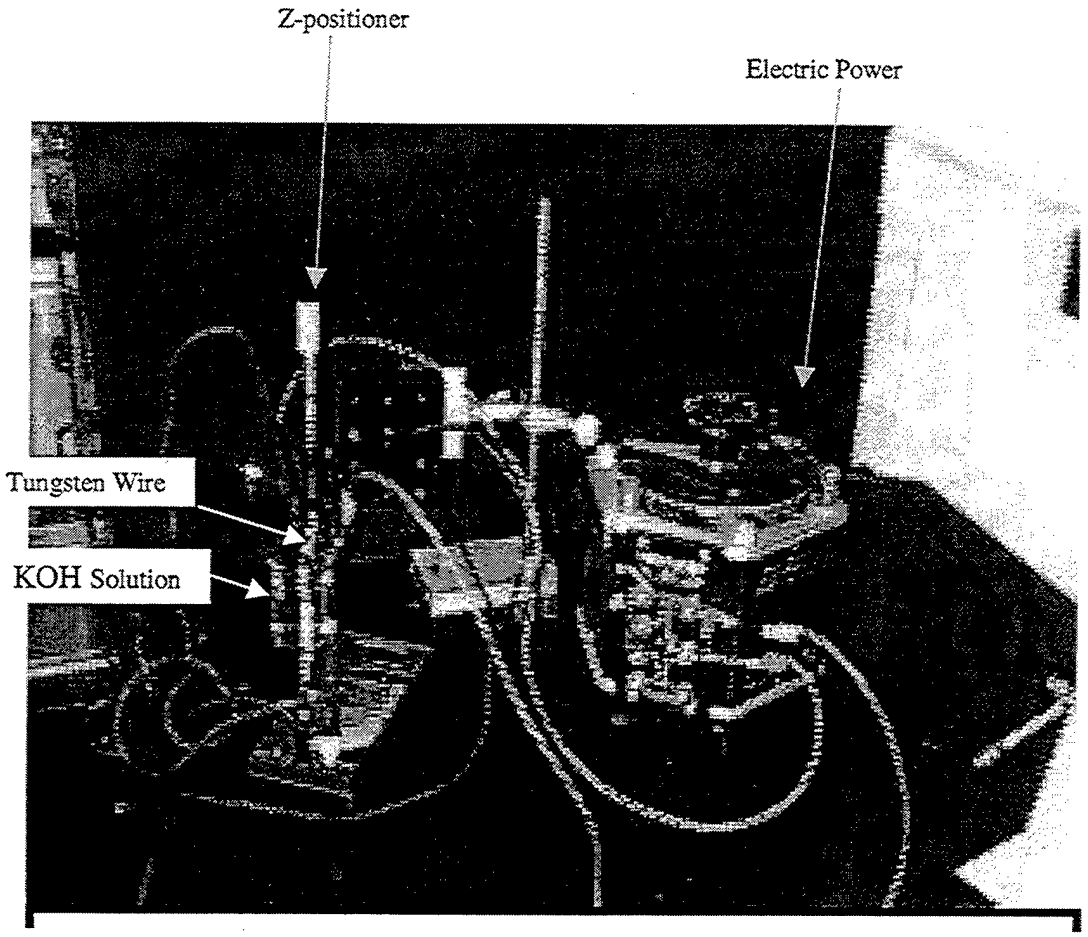

Figure 10 Etching setup for tip preparation. The power supply provided 25V AC at 60Hz. A tungsten wire of 0.015 inch diameter was used as the etched electrode while a palladium wire was used as the counter electrode. The concentration of the potassium hydroxide (KOH) solution was 5moles/litre. The power was turn on for about 4 seconds.

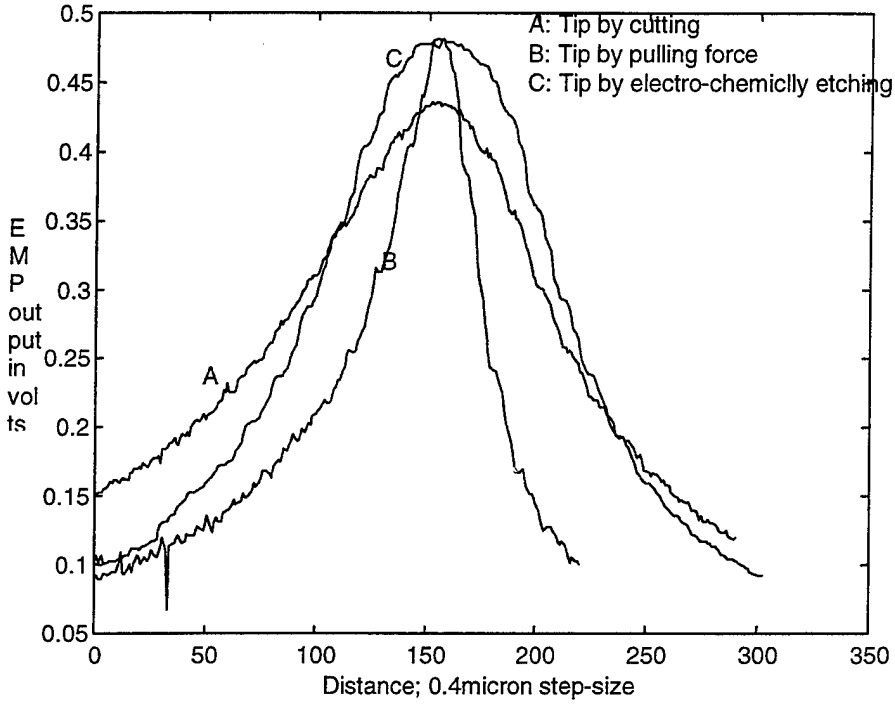

Figure 11 Resolution comparison of different tapered tips. Tips prepared by cutting (A), by pulling force and chemical cleaning (B), and by electro-chemically etching (C) were used. In each case, the probe was scanned over a 25micron-by-125micron rectangular wire along the shorter edge. Each of these scans was performed with the same tip-sample distance of about 20microns.

4. 1. 3 Increase Signal-to-noise Ratio

To improve the signal-to-noise ratio of the EMP system, three techniques have been employed as follows:

a) Synchronized measurement

In a previous version of the EMP, the measurement was performed in the base-band. Noises of all frequencies entered the probe and deteriorated the measured signal, especially very low frequency noises such as the system drifting induced by temperature or mechanical changes. To get rid of the baseband noise while keeping the system's linearity, we employed a synchronous measurement. We made an oscillation table as the sample holder, and let it oscillate at a couple of hundred Hz. A lock-in amplifier is used to pick up the signal at a predetermined frequency. The lock-in amplifier is a very narrow band bandpass filter in nature. Consequently, we modulated the tip-sample distance, performed filtering at the modulated frequency, and therefore got rid of most of the noise, especially the DC drifting.

The oscillation table is supported by 4 speakers sitting at each corner. To make sure this table oscillates evenly (otherwise the real image may be deformed by differences in oscillation at different parts of the sample), the speakers should be of the same oscillation strength, and of the same phase.

One signal source (HP 33120A) is used to drive these four parallel connected speakers, and the mass of the table is evenly distributed so that the phase of oscillation is the same throughout the table. Four potential meters are connected in series with the speakers. They are carefully adjusted to ensure that the oscillation amplitude is the same at every part of the table. We used an optical distance sensor to check the oscillation of the table, and the unevenness was under 3%.

The choice of a modulation frequency is also important. There are several mechanical resonance peaks for the oscillation table. We need to make sure that the modulation frequency is not close to any of those resonance peaks. Otherwise whenever the X-Y stage moves, it would take a very long time for the mechanical oscillation to decay. This oscillation is "seen" by the output as noise. Fig. 12 shows the EMP system noise as a function of modulation frequency.

Fig. 13 shows the comparison of resolution between asynchronized measurement and synchronized measurement. In each case a 125μm metallic wire was scanned. The synchronized measurement gave us a much better result.

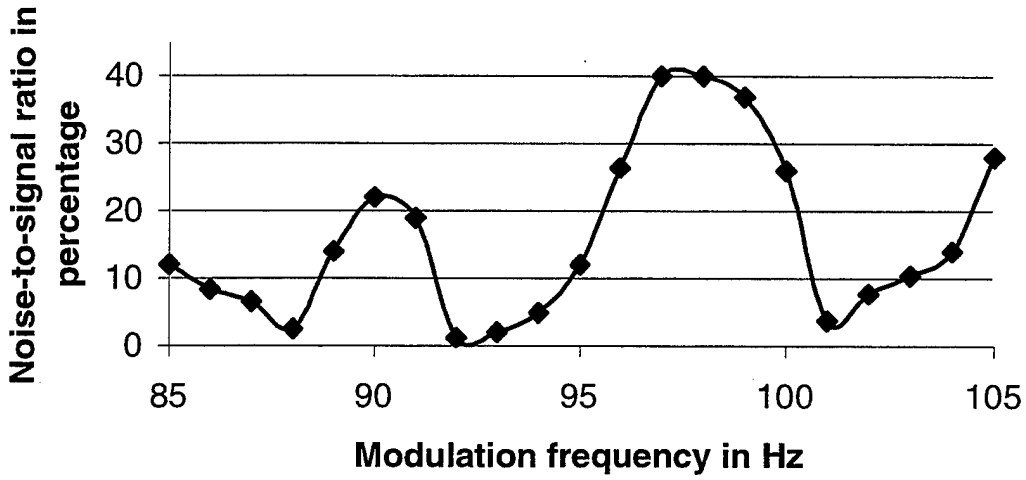

Figure 12 Different modulation frequency results in different signal-to-noise ratio. When the modulation frequency is close to one of the resonant frequencies of the sample-holder, the noise becomes really large.

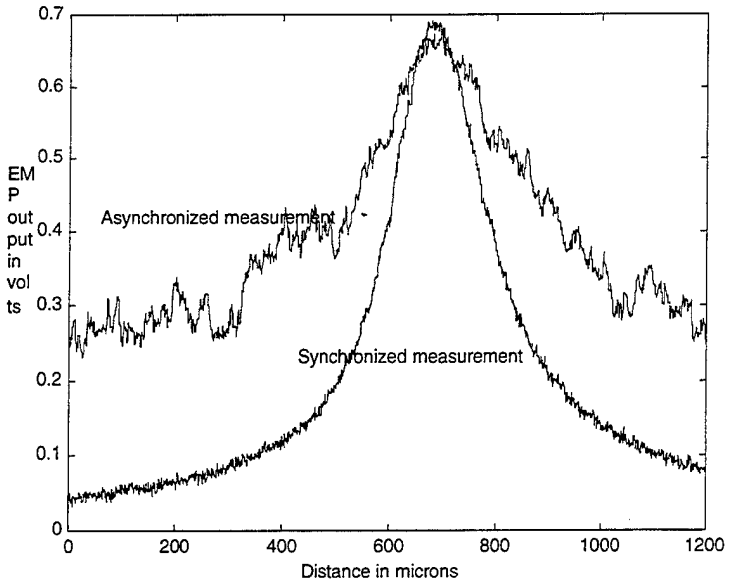

Figure 13 The comparison of synchronized measurement and asynchronized measurement. In each case the probe was scanned over metallic wire of 125micron diameter. Synchronized measurement resulted in a much better spatial resolution.

b) Distance compensation

Fig. 14a shows the tip-sample distance dependence of the EMP output, from which we may clearly see the exponential decay of the evanescent wave. The corresponding SONNET simulation result is shown in Fig. 14b. For higher resolution, the tip should be scanned as close to the sample as possible, because the larger output results in a larger S/N (the system noise has no dependency on distance). The improvement of lateral resolution is easier to understand: for a certain cubic angle, the area of sample "seen" by the tip become smaller. So, decrease the tip-sample distance to a few microns is desirable, and such an accurate positioning needs a fine control system. More importantly, in many applications, it is necessary to disentangle the probe dependence on both conductivity and tip-sample distance.

We introduced a distance compensation scheme to solve these problems. A fiber optic displace sensor (Philtec RC24-L) is the key element of this feedback loop. It is placed right next to the microwave tip to sense to surface height variation, with a 0.05micron resolution. According to this detected signal, the Z-stage stepper motor will adjust the height of the probe in real time to get rid of the topological dependence. As the probe moves very closely along the surface of the sample, the resolution then also improves.

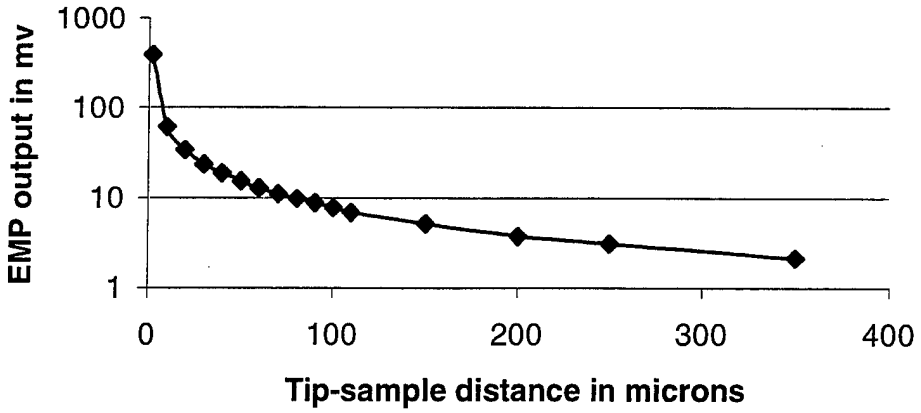

(a)

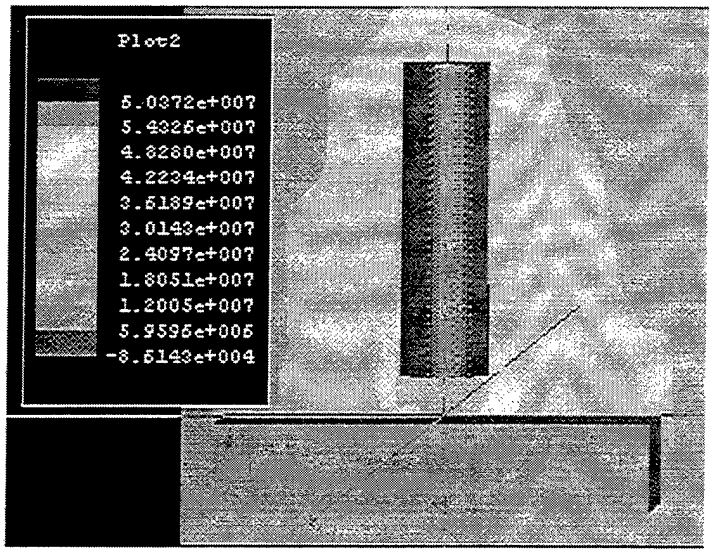

(b)

Figure 14 (a) EMP output as a function of tip-sample distance.
(b) Electric field intensity pattern calculated using finite element method showing the side view of the probe (diameter 10 μm).

c) Choice of operation mode

We have tested two operation methods of EMP imaging: amplitude measurement with fixed frequency, and frequency-shift measurement with fixed amplitude. In the former one, we operate the resonator at a frequency very close to the resonant peak and measure the amplitude of the output. For the second method, we used a feedback circuitry to keep the probe output constant by changing the microwave frequency. Fig. 15 shows the line scan results using both methods. In both cases, a 125micron metallic wire was scanned. As shown on the graph, the amplitude measurement gave us a better resolution, while the frequency measurement might have a linearity advantage.

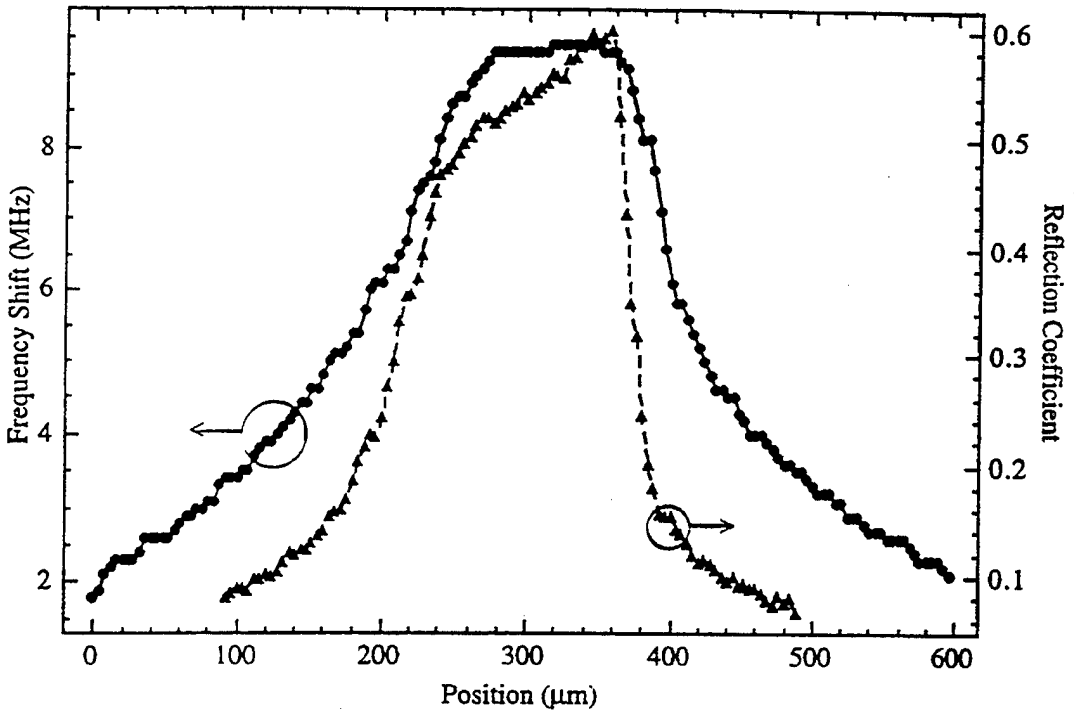

Fig 15 EMP scans of a 125μm object. Two scans were performed to compare the resolution of the frequency-compensated technique with that of the regular asynchronous techique. In the frequency compensated method, the amplitude of the reflected wave was fixed by changing the operation frequency of the EMP. The frequency compensated scans resulted in poorer resolutions.

4.1.4 Testing of the Improved Spatial Resolution

To test the spatial resolution of the EMP system, we chose a micro-electro-mechanic-structure (MEMS) chip as a standard sample. Fig. 16 shows the area that was scanned, which contained features such as 2μm wide straight lines, and 10μm periodic squares. Fig. 17 is a 1D EMP scan of the 2μm straight line. It is obtained by scanning the probe over the straight line back and forth in the y direction without any motion in the x direction. The full width at half maximum (FWHM) of the 2μm line is 2.6μm, while the minimum detectable signal (MDS), which is defined by unit S/N, is smaller than 0.4μm. The two-dimensional EMP image of the line is shown in Figure 18a, while the optical image and STM image of that line are presented in Figure 18b and Figure 18c, respectively. Finally, the EMP image, optical image, and STM image of the periodic squares are show in Fig 19a, 19b, and 19c for comparison. On the STM image, only the edge of the periodical area is show, because the Instructional STM (Burleigh^{TM}) has a maximum scanning range of 7μm * 7μm. During all of the scanning, the EMP was operated at 965MHz, and the tip was kept at 2μm above the sample. The STM was operated at a constant-distance mode.

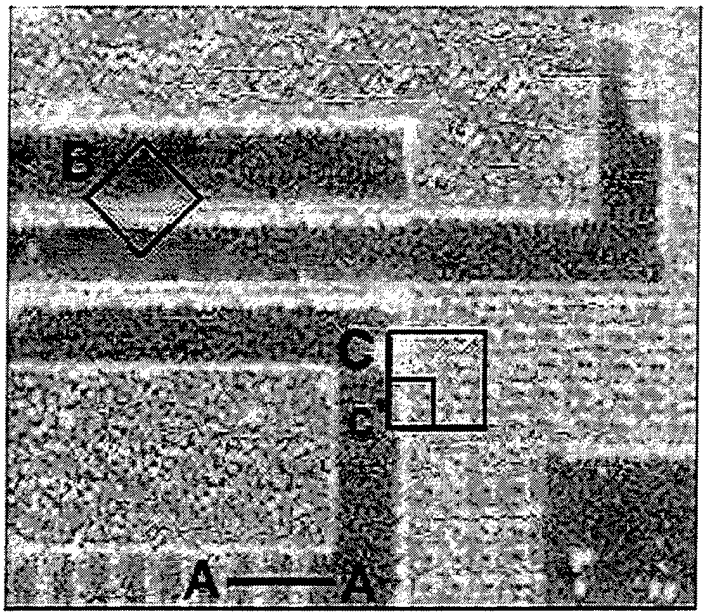

Figure 16 The optical image (for registration purpose) of several structures on a MEMS chip. These structures were scanned with EMP and scanning tunneling microscope (STM).

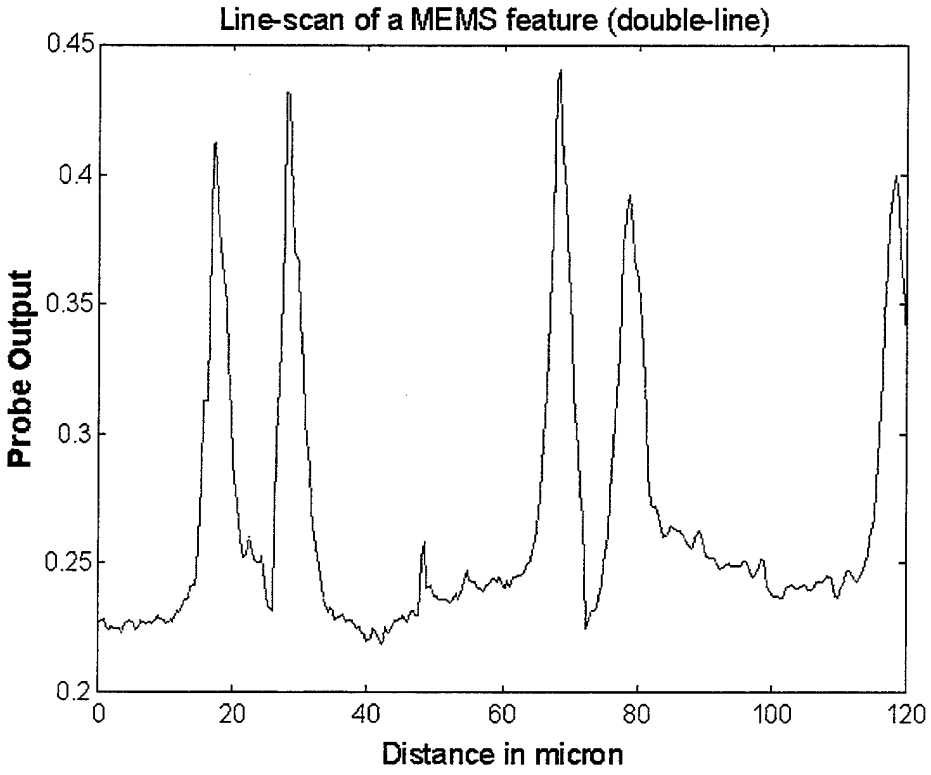

Figure 17 The one-dimensional EMP-scan of a double-line feature (shown in Figure 4 as area A-A'). The EMP scanned over those two lines back and forth. This figure shows the reproducibility of our measurement.

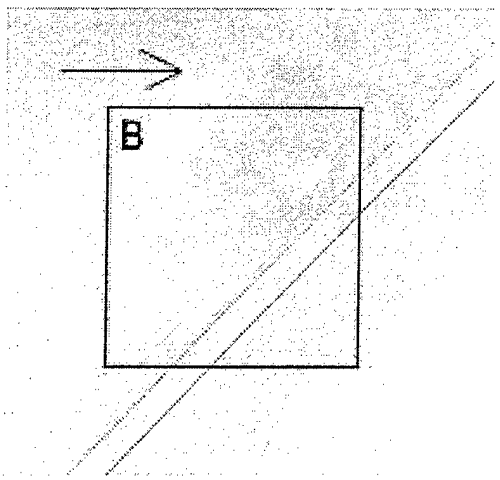

(a)

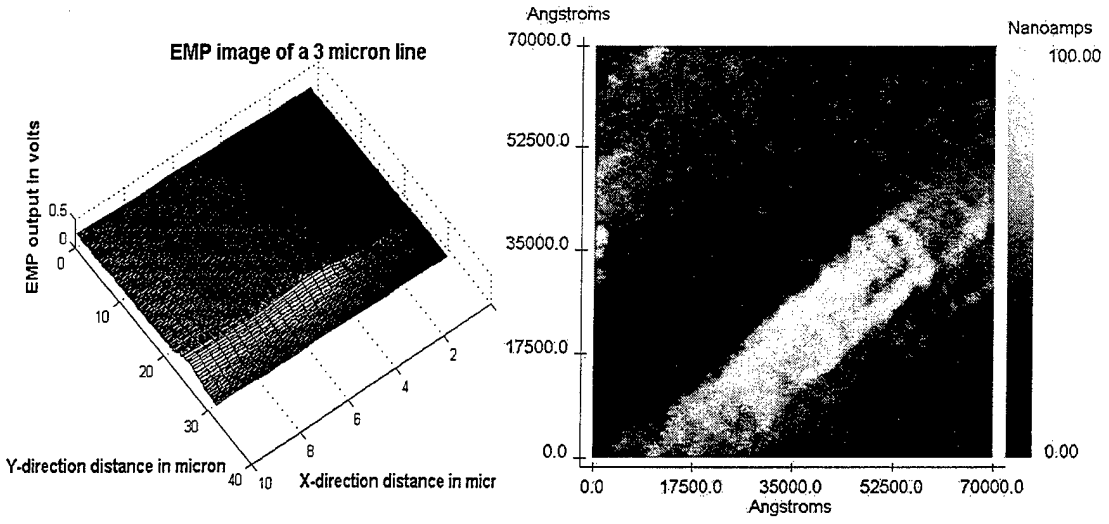

(b) (c)

Figure 18 The optical image (a), EMP image (b), and STM image (c) of a 2μm straight line (shown in Figure 16 as area B).

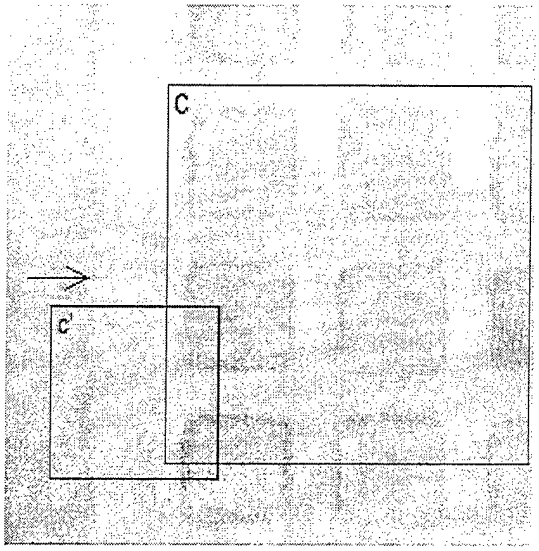

(a)

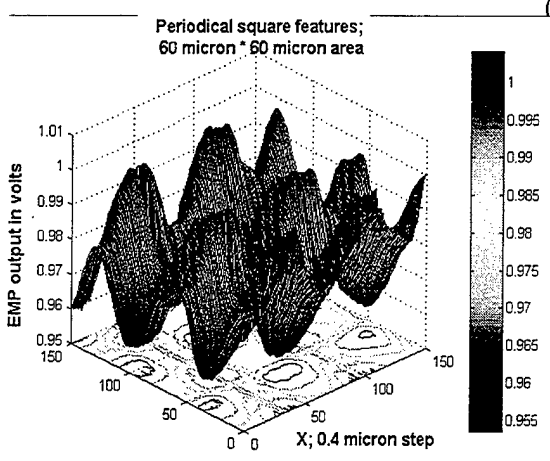

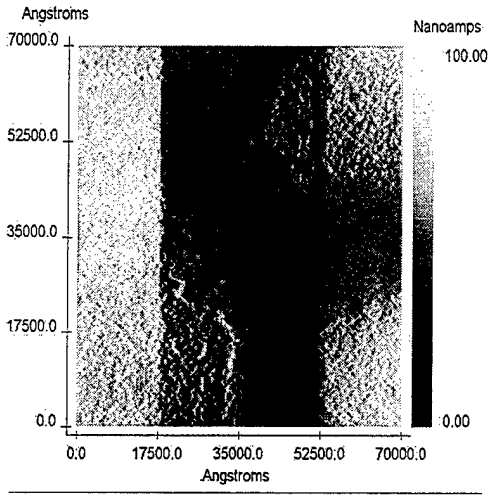

(b) (c)

Figure 19 The optical image (a) and the EMP image (b) of a 10μm square features (Area C in Figure 16). The STM image (c) shows the roundness at corners of those squares (Area c' in Figure 16).

4.2 Control System Improvement

4.2.1 Position Registration

Currently, a piezo-electric XYZ stage is under-construction for better positioning and registration.

4.2.2 Scanning Speed

In a previous EMP system, a digital multimeter was used to convert the analog signal into a digital signal before sending it to the computer. Because of the very low speed of the A/D conversion, the scanning rate was about 1Hz/point. In our current setup, a DAQ board from National Instrument is in use for data acquisition and motor control. Because of its high performance, the scanning rate of the EMP system has been improved to 8~10 Hz/point. In the meanwhile, a multi-sampling technique can be performed for a better signal to noise ratio.

4.2.3 Graphic Interface

LabView is currently used as our operating platform. In contrast to the previous QBasic environment, LabView has a complete instrument library and has a high level graphic programming platform, which makes programming and parameter modification very easy.

Fig. 20 shows a typical virtual instrument front panel for 2D scanning.

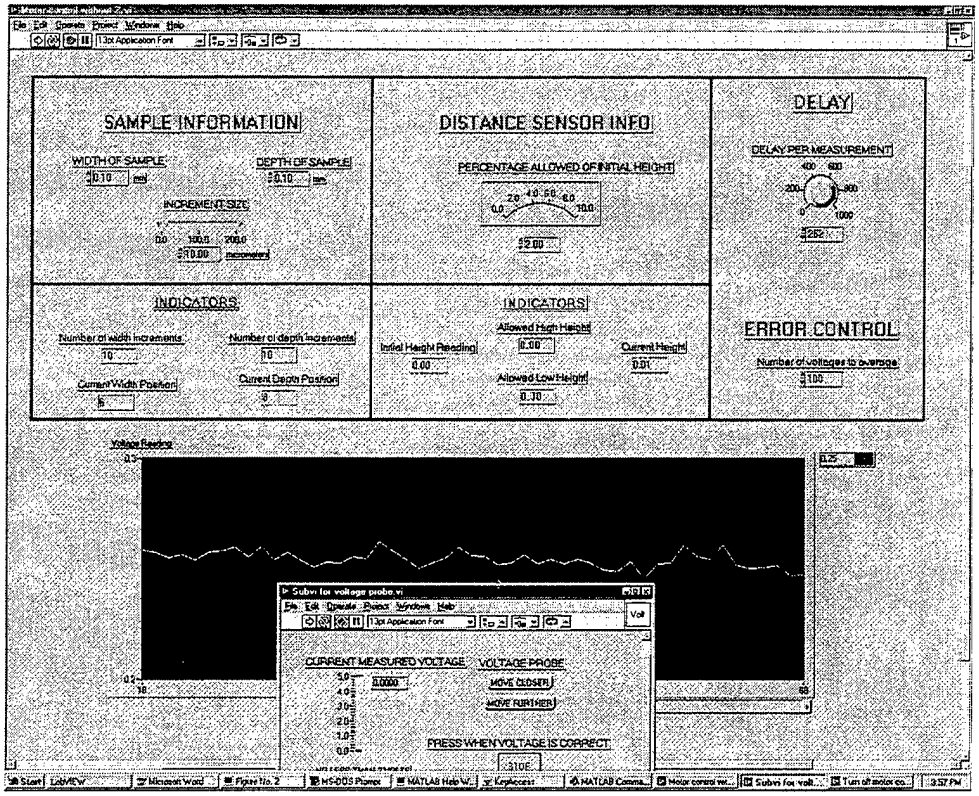

Figure 20 Typical LabView virtual instrument front panel.

5 Probe Calibration

In this chapter, techniques used to perform the probe calibration are discussed.

5.1 Calibration of Sheet-Resistance Measurement Using Standard Samples

To perform quantitative mapping of conductivity, we calibrated the probe over a large range of sheet resistance (0.24Ω/□ to 65kΩ/□). In our experiment, we used a Signatone 4-point probe, together with a Keithley 182 Sensitive Digital Multimeter and 202 Programmable Current Source to measure the sheet resistance of different samples. With this highly sensitive setup, a change of 10^{-4} in surface resistance can be detected, and the deviation was below 2%. The EMP was then used to measure the microwave resistivity of these samples. For each sample, the fiber optic sensor was used to adjust the probe-sample distance to be exactly 2μm to ensure the reproducibility. Silicon wafers with different doping levels were used as the calibrating samples, not only because they offer a large range of sheet resistances, but also because they have an optical-smooth surface, and nearly identical surface reflectance from sample to sample. Fig. 21 shows the calibration results. One can see that monotonous change of the EMP output with the change of sample surface resistance. The accuracy of our measurement was better then 6% for samples of low resistivity, and became worse (50% off) for high resistance sample. This is expected since it is well known that a 4-point-probe is not suitable for measuring high resistance sample.

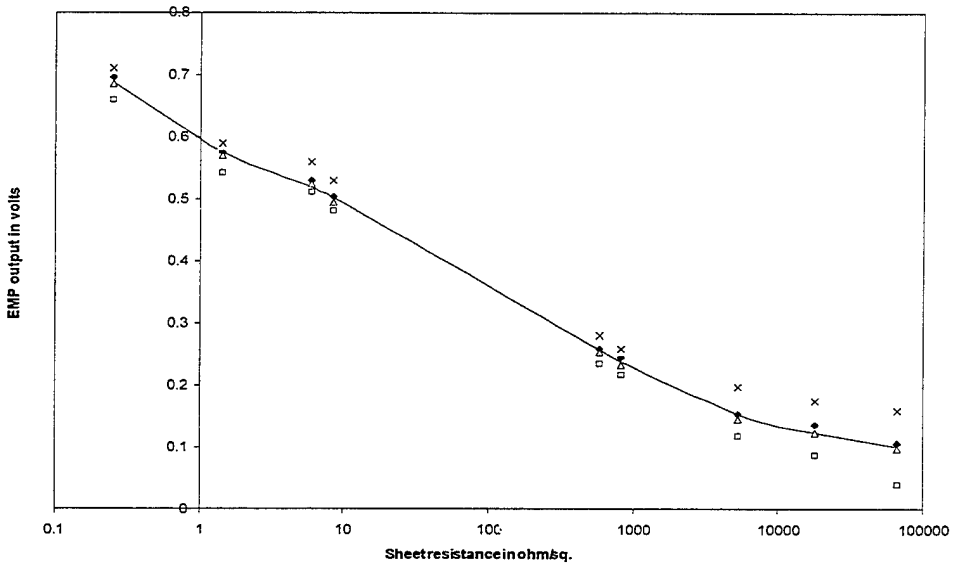

Figure 21 Calibration of conductivity measurement using standard samples. The samples we used ranging from 0.24Ω/□ to 65KΩ/□. Four groups of nearly identical measurements, indicated by different legends in the figure, were performed to obtain the err-bar. The main sources of variations in the signal in these measurements is the environmental parameters such as temperature variations, and drifts in the electronics.

5.2 Calibration of Sheet-Resistance Measurement Using Optical Method

The previous method used one standard sample at a time to obtain one set of calibration data. The main problem associated with this method is that we have to mount a different sample every time, and the change in the probe-sample distance and sample surface reflectance contribute to the experiment error. In addition, it is prohibitive to obtain enough standard samples of various conductivity over a large range along with very small differences for calibration purposes.

To solve these problems, another technique was used and gave us fine calibration for a certain range of resistance. Instead of using many different samples, only one lightly doped silicon wafer was used. We first performed the 4-point-probe measurement while lights of different intensity were shone onto the wafer, and each time the sheet resistance was recorded. When the EMP measurement was performed, we again shone lights on the wafer, one at a time, and each time the light intensity was exactly duplicated. This method confirmed that the EMP outputs matched the 4-point-probe outputs. Fig. 22 shows the EMP output as a function of sample sheet-resistance. In this smaller calibrated range, the EMP output changes more or less linearly with sample sheet resistance. On the contrary to the previous technique, this calibration technique is only applicable for high resistance sample, because strong shining light heats the sample. Consequently, this rise in temperature results in output drifting.

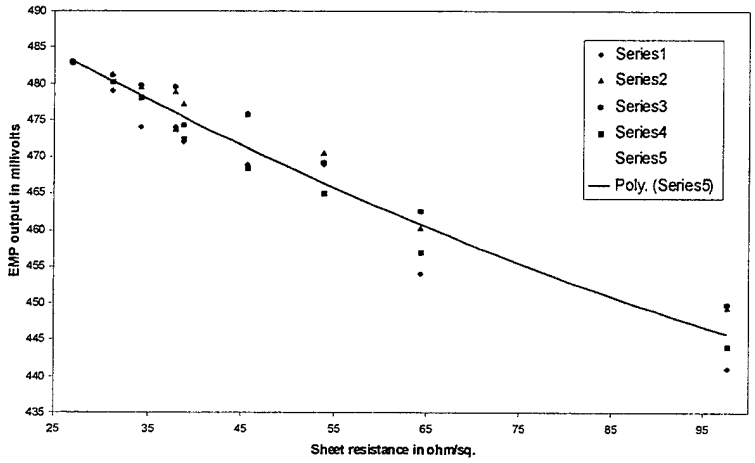

Figure 22 Calibration of conductivity measurement using optical method. We used a lightly doped silicon wafer and shone lights of different intensity on it. Each time the sheet resistance was measured using 4-point-probe, and matched to the corresponding EMP output (of the same shone light). Four groups of nearly identical measurements, indicated by different legends in the figure, were performed to obtain the err-bar. The main sources of variations in the signal in these measurements is the environmental parameters such as temperature variations, and drifts in the electronics.

5. 3 Calibration of Dielectric Constant Measurement

In addition to sheet resistance mapping, we also calibrated our probe for quantitatively mapping of dielectric constant. Fig.23a shows the maximum EMP output dependence on the relative dielectric constant of materials, while Fig. 23b shows the EMP output change verses the dielectric constant change when the sample-probe distance was fixed at 20microns. Fig. 24 shows a two-dimensional map of the dielectric regions next to each other, each 1mm wide. The first large peak is obtained for a region (Duroid) with dielectric constant of 11.8. The second peak is contributed by a region of 5.5 relative dielectric constant, while the third layer detected as the third peak is a region of 3.6 relative dielectric constant. The minimum detectable change in relative dielectric constant is calculated to be 1.7% (by MDS definition).

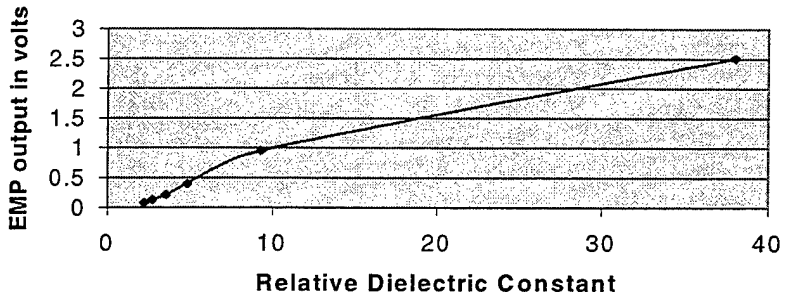

(a)

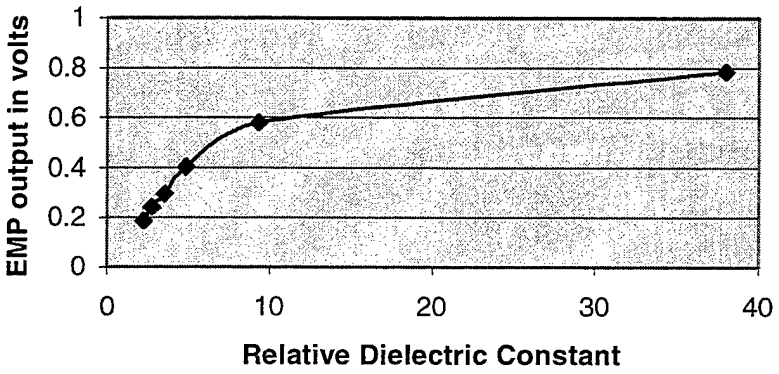

(b)

Figure 23 Calibration of relative dielectric constant, with a tip-sample distance of 0.4micron (a) and 20microns (b) respectively.

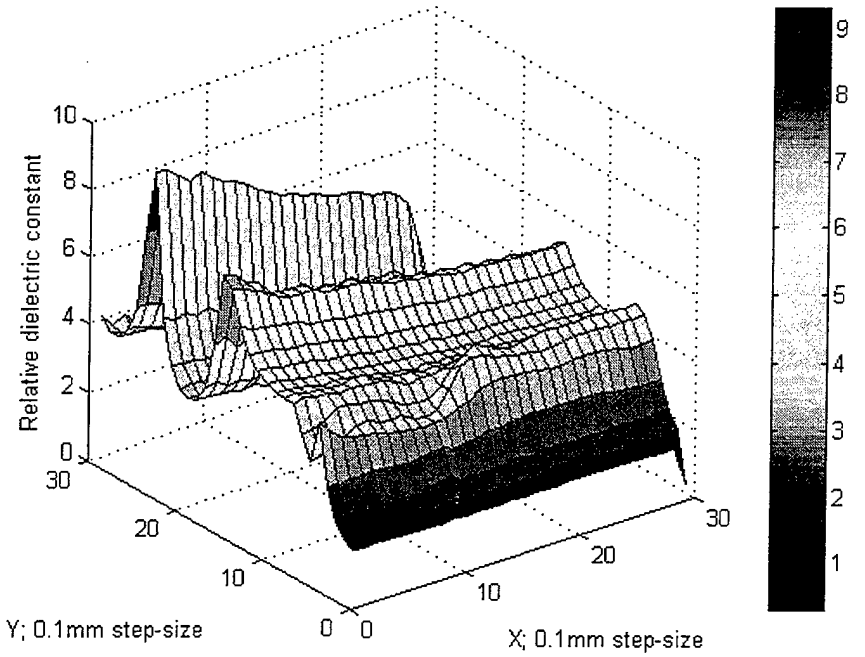

Figure 24 Synchronous scan of dielectric layers of different relative dielectric constant. The first peak from left is due to a layer with ε_r=9.3, the second peak due to a layer with ε_r=4.8, and the third peak due to a layer with ε_r=2.2.

6 Material Characterization

Various kinds of materials have been imaged and/or characterized by the evanescent microwave probe. The results are presented in this chapter.

6.1 Insulators

Fig. 25 shows the synchronous scan of a Boron Nitride film. The film is optically smooth, with no visible dents or bumps. Using the microwave probe, one can clearly see the dielectric constant variation over different areas of the film. The clusters that have a relatively low dielectric constant are of size between 100 microns to 400 microns. This scan was performed with about a 10μm probe-to-sample distance.

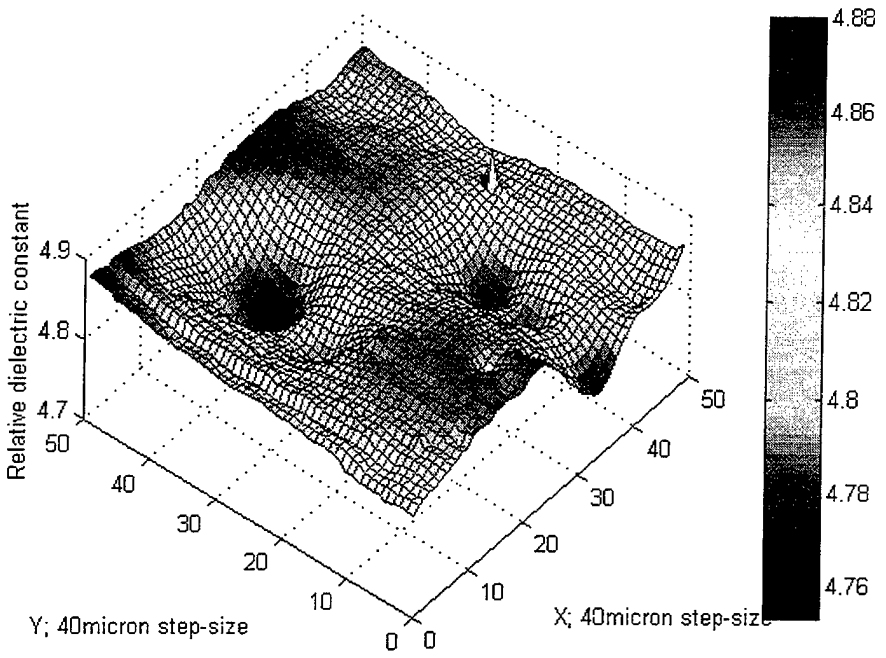

Figure 25 Non-uniformity of dielectric constant in a Boron Nitride sample. The ε_r of the Boron Nitride film varies from 4.76 to 4.88. The typical size of those clusters with relatively lower ε_r is 200-400 microns.

Fig. 26 shows the optical image (a) and the EMP image (b) of a polymer sample. Since the sample was transparent, there were no visible strips. The optical image, showing the thickness variation of the film sample, was obtained using an optical spectrometric method by Wright Patterson Air Base. From the EMP image, and the corresponding optical image (the upper-half), one can clearly see the similarity between these two images. When we scanned over a smaller area (0.1mm * 0.1mm), we also detected the surface roughness information (Fig. 26c). In generating Fig. 26b and Fig. 26c, a two-dimensional moving average filter and Wiener filter were used to obtain a better image.

Fig. 27a shows the optical image of a V-shaped micro-groove under an optical microscope, while Fig. 27b shows the EMP image of the same structure. These figures demonstrate the EMP's ability to image topological change.

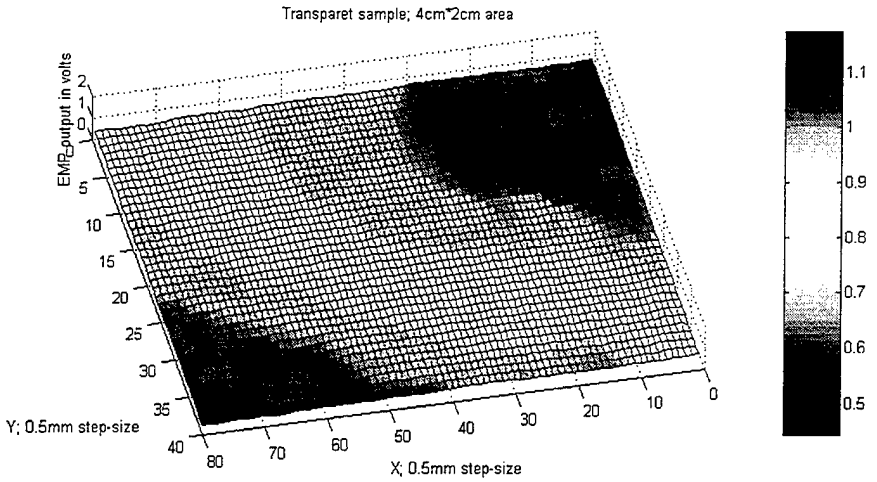

(a)

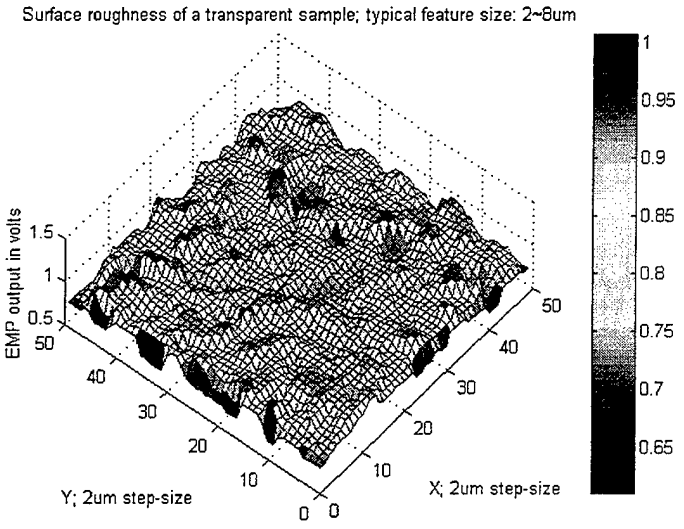

(b)

Figure 26 The variations in thickness (a) and surface roughness (b) of a polyester film sample.

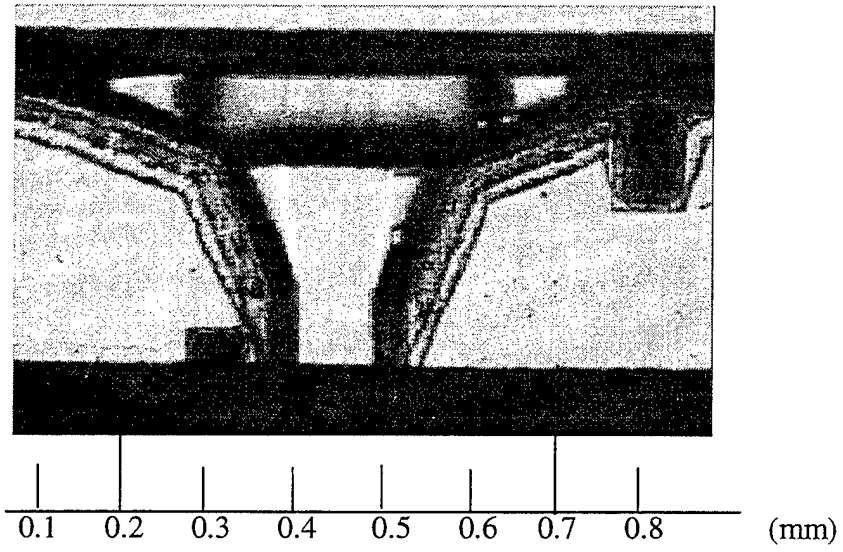

(a)

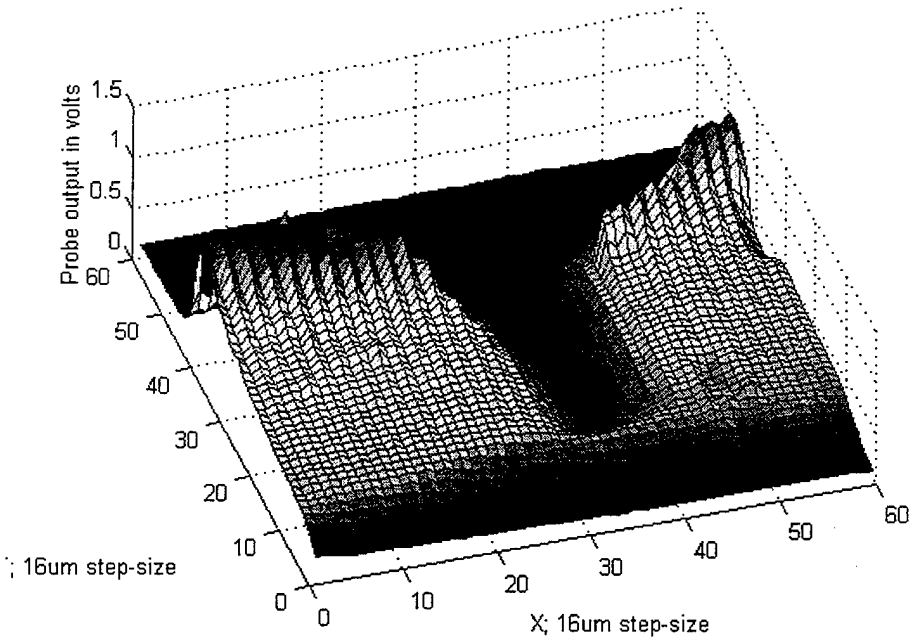

(b)

Figure 27 The optical image (a) and evanescent microwave image (b) of a V-shaped groove.

6.2 Semiconductors

Fig. 28 shows the optical image (a) and EMP image (b) of a MEMS structure. The "bumps" on these figures are deposited polysilicon. The substrate is lightly doped silicon.

Fig. 29a shows the optical image of a $YBa_2Cu_3O_{7-\delta}$ thin film on a Lanthanum Aluminate substrate, and Fig. 30.b shows the corresponding EMP image. Along with many similarities, there are also some differences. These differences result from the fact that visible light and microwaves have different penetration depths.

Fig. 30 is a photograph of a waveform on an oscilloscope. To investigate the optical property of semiconductors, we shone a light, modulated with a frequency of ~10Hz, on a lightly doped silicon sample while we observed the EMP output on the oscilloscope. From this waveform we can derive the carrier re-combination time of the semiconductor. Typical lifetimes that were measured were with order of 5-8ms. The detection system that was used in this measurement consisted of an amplifier with 10kHz (0.1ms response time) bandwidth. The oscilloscope directly shows the output of the amplifier.

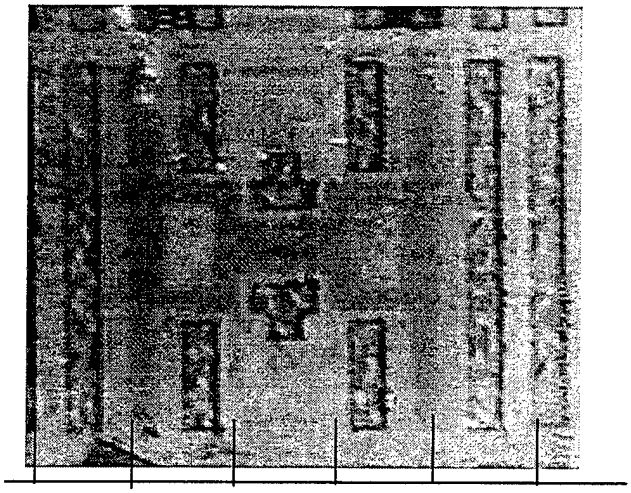

0.2 0.4 0.6 0.8 1.0 1.2 (mm)

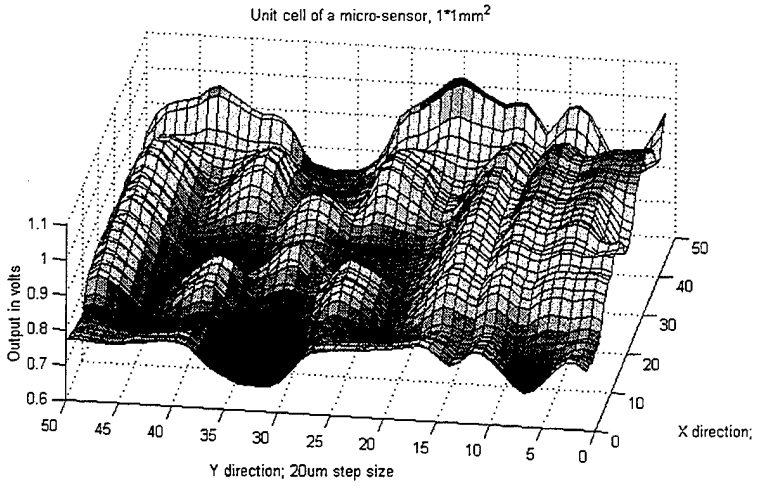

(b)

Figure 28 Optical image (a) and evanescent microwave image (b) of a MEMS structure.

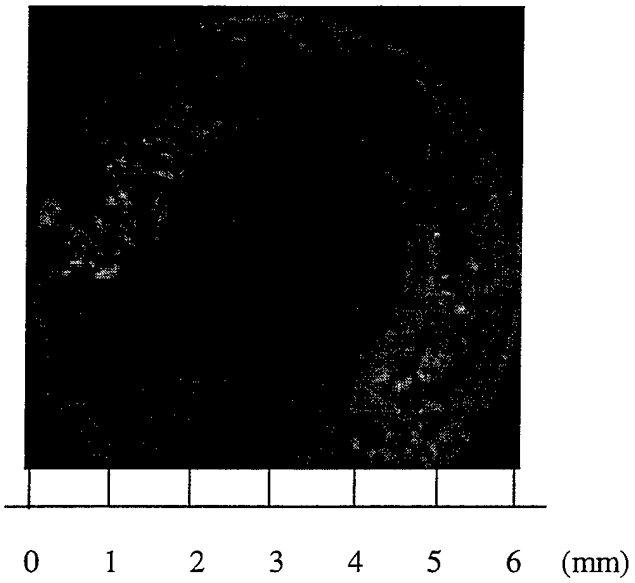

(a)

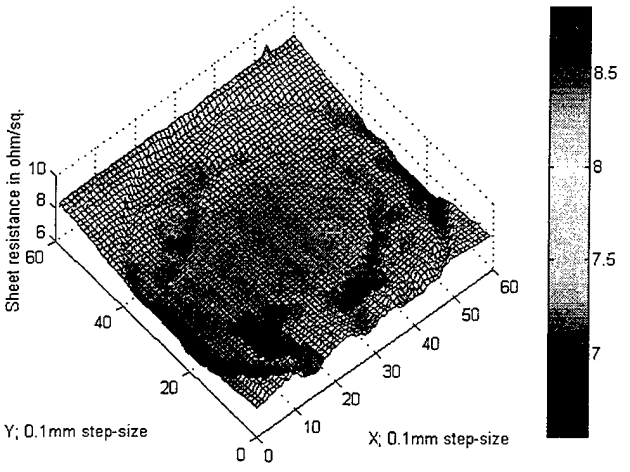

(b)

Figure 29 Optical image (a) and EMP image (b) of a$YBa_2Cu_3O_{7-\delta}$ thin film on Lanthanum Aluminate substrate. The variations of colors on the EMP image correspond to the change of sheet resistance.

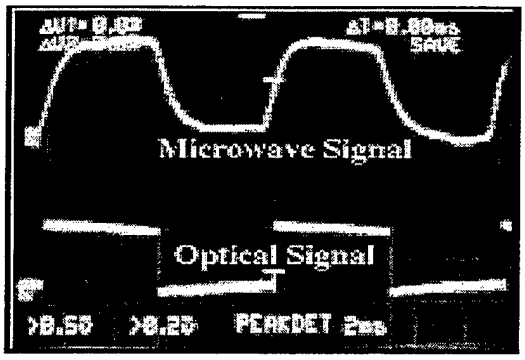

(a)

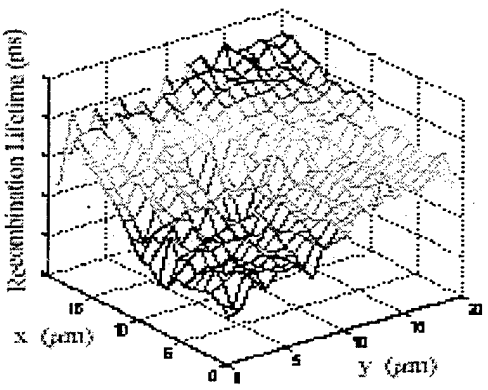

(b)

Figure 30 (a) Carrier lifetime measurement using the EMP. A switched optical pulse generated by a GaAs laser diode was used to shone on a silicon sample, and the EMP output response was recorded as the oscilloscope trace. The carrier recombination lifetime can be calculated from the transient behavior of EMP output when the optical pulse is turned off. (b) The recombination lifetime may be obtained by moving the microwave probe around with silicon sample to different locations and measuring the fall-time (which is proportional to the recombination life time) from the oscilloscope.

6.3 Metals

Fig. 31 shows a scratch on a copper plate. We can see the details of the trauma, which are important in studying deformation, fatigue, or welding junctions of metals.

Fig. 32 was obtained by a synchronous scan of copper disks embedded in a duroid layer with a dielectric constant of 5.5. The largest peak corresponds to a copper disk of 1mm in diameter while the smallest peak corresponds to a copper disk of 40micron in diameter.

Fig. 33 shows both the optical image (a) and the EMP image (b) of a "CWRU" medallion. Both the resolution and the contrast of the EMP are comparable to those of the optical image.

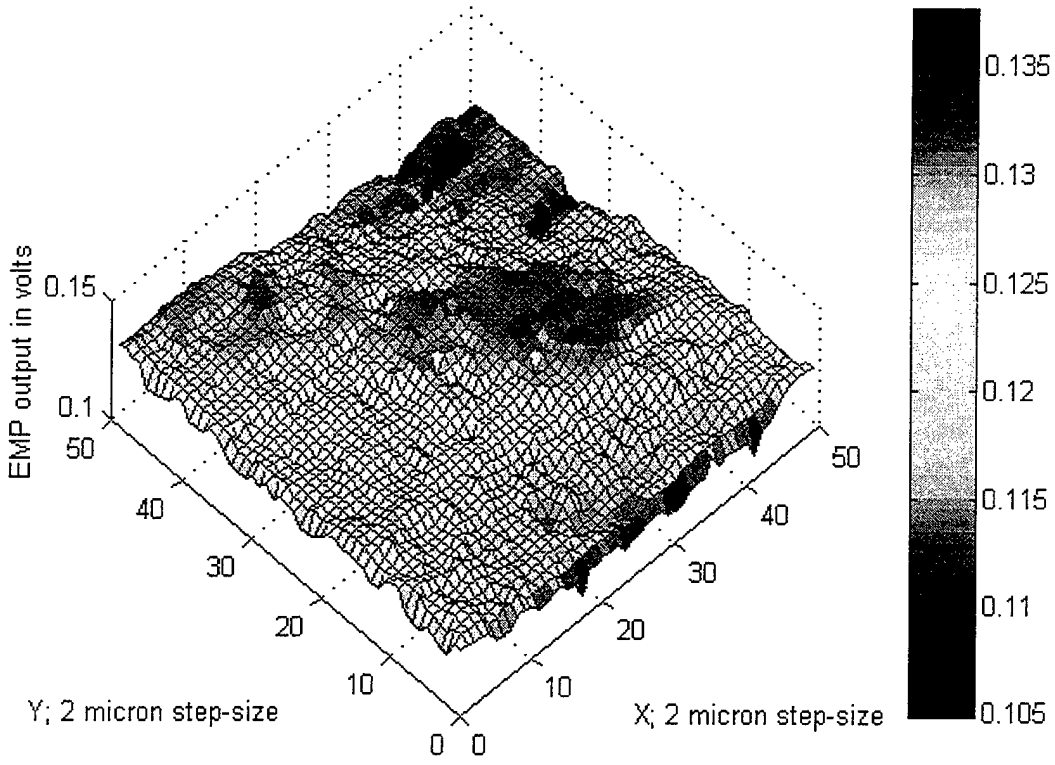

Figure 31 A scratch on a copper sample was scanned by EMP.

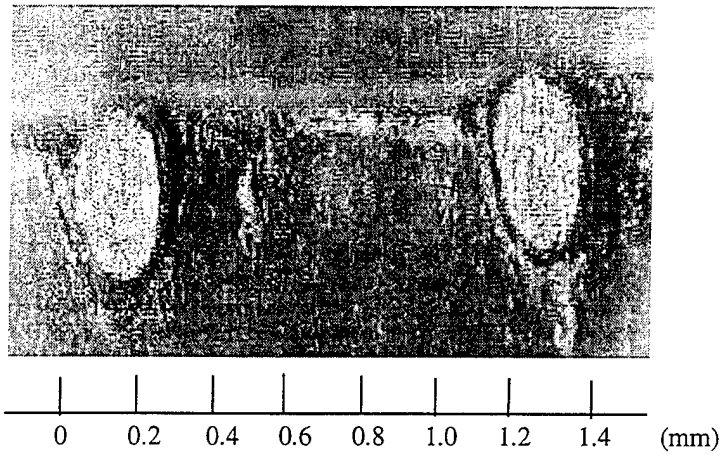

(a)

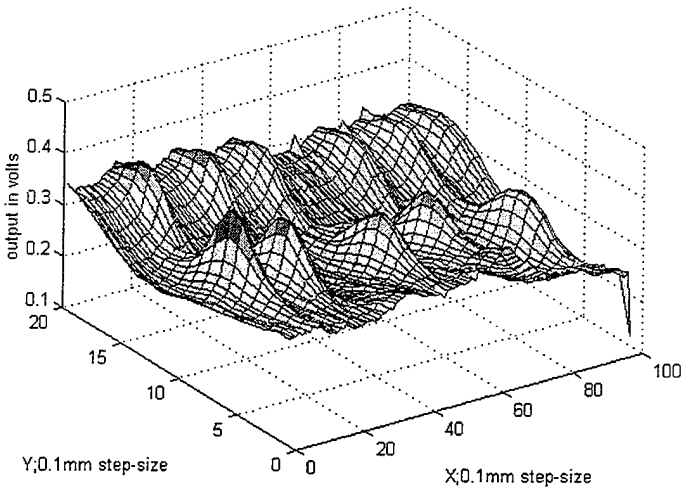

(b)

Figure 32 Optical image (a) and EMP image (b) of metallic disks embedded in a dielectric layer of ε_r=5.5. The largest peak corresponds to a copper disk of 1 mm diameter while the smallest peak is obtained for a copper disk of 1/40 mm (25 μm) diameter.

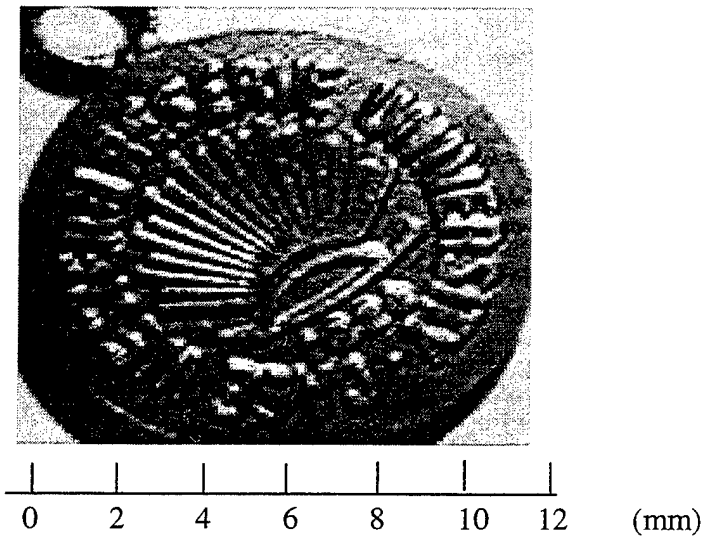

(a)

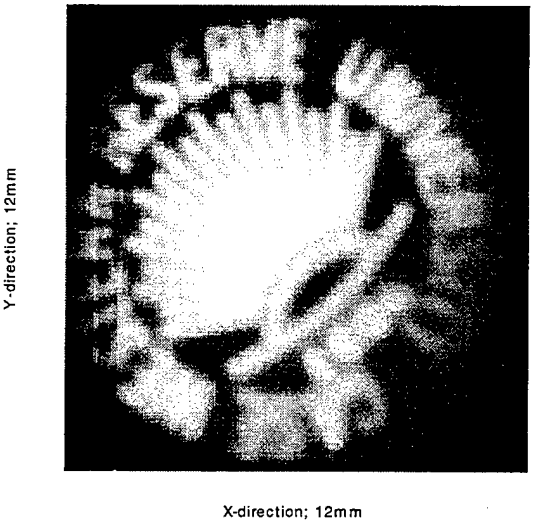

(b)

Figure 33 Optical image (a) and EMP image of a CWRU medal.

6.4 Biological Specimens

Fig. 34 and Fig. 35 show the scanned images for a tooth sample and a leaf sample, respectively. These figures demonstrate the possibility of using the evanescent microwave probe for studying the variations in the physiological state of bio-tissues. These variations result from either a change in the dielectric properties or a change in the relative microwave permitivity.

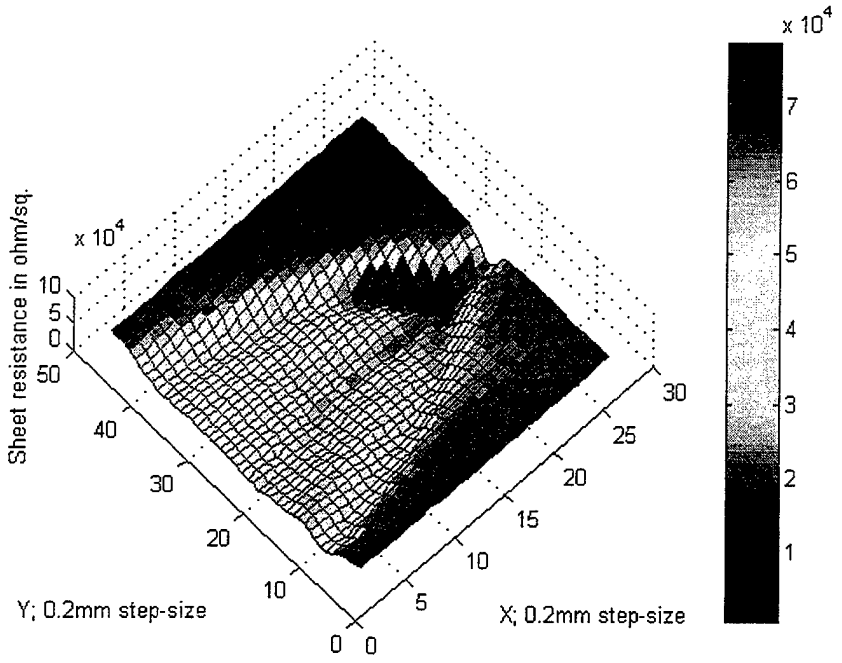

Figure 34 Evanescent microwave image of a half-dried leaf sample. By assuming the change of conductivity dominates, we obtained quantitative mapping of sample sheet resistance, which ranged from 400Ω/ to 8kΩ/ .

(a)

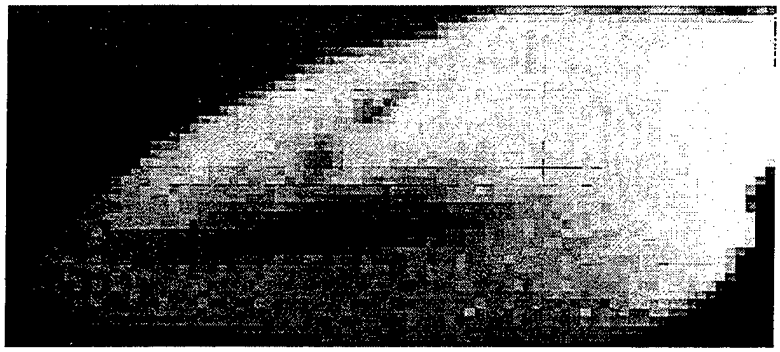

(b)

Figure 35 Optical image (a) and evanescent microwave image (b) of a tooth sample.

7 Conclusion

This work involved systematic design and development of an evanescent microwave probe. A device model was set up and used to study the crucial problems that determine the probe's resolution. Guided by the theoretical analysis, several novel design improvements were made and their effects on improving the performance were documented in contrast with those of the previous probe's setup.

In this work, the output of the probe was calibrated for quantitatively measuring conductivity as well as the dielectric constant of the scanned samples. With the calibrated probe, a large variety of materials ranging from dielectrics, semiconductors, metals, to biological specimens were scanned, and the results were presented. The usefulness of EMP as a material characterization tool was further ascertained.

Finally, further improvements in resolution can be achieved by:

a) Using a piezoelectric scanner in combination with mechanical stepper motors for fine positioning.

b) Operating the probe at a much lower frequency (i. e., at 1GHz when the prime frequency is 10GHz), instead of using a secondary fiber optical sensor, for sample-probe distance compensation. This will ensure that there is no displacement between the conductivity probe and the distance probe.

c) Developing a technique to vibrate the tip of the EMP instead of the sample holder. This way the unevenness of the oscillation can be eliminated.

d) Using magnetic dipole probe for mapping conductivity change in metal. Magnetic dipole probe has advantage over electric dipole probe in better impedance matching for metallic sample.

8 Reference

[1] Memmert, U., Hodel, U. and Hartmann, U., "Combined Ultrahigh Vacuum Scanning Tunneling Microscope Scanning Electron Microscope System", Rev. of Sci. Instrument, 67(6), June 1996, pp. 2269-73.

[2] Mou, J., Yang, J. and Shao, Z., "An Opticaldetection Low Temperature Atomic Force Microscope at Ambient Pressure for Biologicalresearch", Rev. Sci. Instrument. 64(6), June 1993, pp. 1483-9.

[3] Durig, U., Pohl, D. W. and Rohner, F., "Near-field Optical-scanning Microscopy", J. Appl. Phys. 59(10), 1986, pp. 3318-27.

[4] Stephenson, R. J., "A Near-field Optical Microscope with Normal Force Distance Regulation", Rev. Sci. Instrument. 67(11), November 1996, pp. 3891-7.

[5] Noma, T., and Iida, A., "Surface Analysis of Layered Thin films Using a Synchrontron x-ray Microbeam Combined with a Grazing-exit Condition", Rev. Sci. Instrument. 65(4), April 1994, pp. 837-843.

[6] Wegendt, K., Huebener, R. P., Gross, R., Trauble, Th., Geweke, W., Patzwaldt, W., Prusseit W., and Kinder, H., "Eddy Current Technique for Testing Large-area, High T_c Superconducting Films with High Spatial Resolution.", Cryogenics, 35(3) (1995), pp 155-160.

[7] Ylitalo, J., "A Fast Ultrasonic Synthetic Aperture Imaging Method: Application to NDT", Ultrasonics, 34 (1996), pp. 331-333.

[8] Ash, E. A. and Nicholls, G., "Super-resolution Aperture Scanning Microscope", Nature 237, 1972, pp. 510-512.

[9] Steinhauer, D.E., Vlahacos, C. P., Dutta, S. K., Wellstood, F. C., and Anlage, S. M., "Surface Resistance Imaging with a Scanning Near-field Microwave Microscope." Appl. Phys. Lett. 71 (12) pp.1736-1738 (1997).

[10] Lukosz, W., Imagery with Evanescent Waves, Workshop on Unconventional Imagery (SPIE, Bellingham, WA, 1984), p. 73.

[11] Lu, Y., Wei, T., Duewer, F., Lu, Y., Ming, N.-B., Schultz, P., and Xiang, X.-D., "Nondestructive Imaging of Dielectric-Constant Profile and Ferroelectric Domains with a Scanning-Tip Microwave Near-Field Microscope." Science 276(27), June 1997, pp. 2004-2006.

[12] Wei, T. and Xiang, X.-D., "Scanning Tip Microwave near-field microscope." Appl. Phys. Lett. 68(24), 10 June 1996, pp. 3506-3508.

[13] Vlahacos, C. P., Black, R., Anlage, S., Amar, A., and Wellstood, F., "Near-field Scanning Microwave Microscope with 100μm Resolution.", Appl. Phys. Lett. 69(21), 18 November 1996, pp. 3272-3274.

[14] Tabib-Azar, M., Shoemaker, N., and Harris, S., "Superresolution Characterization of Microwave Conductivity of Semiconductors." IOP Meas. Science, Techn., 3, pp. 583-590 (1993).

[15] Tabib-Azar, M., Pathak, P., Ponchak, G., "Non-Destructive Super-Resolution Imaging of Defects, Non-uniformities, and Residual Stress in Metals, Composites, Semiconductors, and Dielectrics Using Evanescent Microwaves." Rev. of Sci. Instrument.

[16] Pathak, P., Tabib-Azar, M., and Ponchak, G., "An Evanescent Microwave Probe for Super-Resolution Nondestructive Imaging of Metals, Semiconductors, Dielectrics, Composites and Biological Specimens." 1998 Conference of Non-Destructive Testing, Anaheim, California, 1998.

[17] Pathak, P., Super-Resolution Evanescent Microwave Imaging of Materials. MS Thesis, Case Western Reserve University (1998).

[18] Tabib-Azar, M., Su, D.-P., LeClair, S., and Ponchak, G., "The Ultimate Resolution of Super-Resolution Imaging Using Evanescent Microwave Probes." Rev. of Sci. Instrument.

[19] Collin, R. E., Field Theory of Guided Waves. IEEE Press, New York, 2nd edition (1991).

[20] Ramo, S., Whinnery, J. R. and Van Duzer, T., Fields and Waves in Communication Electronics, New York, 2nd edition (1984).

[21] Bethe, H. A., "Theory of Diffraction by Small Holes." Phys. Rev., 66(7), pp. 163-182 (1994).

[22] King, R. W. and Smith, G. S., Antennas in Matter The MIT Press, Cambridge, pp. 196-239 (1981).